JOURNAL OF GEOPHYSICAL RESEARCH: ATMOSPHERES, VOL. 118, 1777–1803, doi:10.1029/2012JD018136, 2013

Inorganic and black carbon aerosols in the Los Angeles Basin during CalNex

J. J. Ensberg,[1] J. S. Craven,[1] A. R. Metcalf,[2] J. D. Allan,[3,4] W. M. Angevine,[5,6] R. Bahreini,[7] J. Brioude,[5,6] C. Cai,[8] H. Coe,[3] J. A. de Gouw,[5,6] R. A. Ellis,[9] J. H. Flynn,[10] C. L. Haman,[10] P. L. Hayes,[5,11] J. L. Jimenez,[5,11] B. L. Lefer,[10] A. M. Middlebrook,[6] J. G. Murphy,[12] J. A. Neuman,[5,6] J. B. Nowak,[5,6] J. M. Roberts,[6] J. Stutz,[13] J. W. Taylor,[3] P. R. Veres,[14] J. M. Walker,[15] and J. H. Seinfeld[1,15]

Received 22 May 2012; revised 4 December 2012; accepted 10 December 2012; published 19 February 2013.

[1] We evaluate predictions from the Community Multiscale Air Quality (CMAQ version 4.7.1) model against a suite of airborne and ground-based meteorological measurements, gas- and aerosol-phase inorganic measurements, and black carbon (BC) measurements over Southern California during the CalNex field campaign in May/June 2010. Ground-based measurements are from the CalNex Pasadena ground site, and airborne measurements took place onboard the Center for Interdisciplinary Remotely-Piloted Aircraft Studies (CIRPAS) Navy Twin Otter and the NOAA WP-3D aircraft. BC predictions are in general agreement with observations at the Pasadena ground site and onboard the WP-3D, but are consistently overpredicted when compared to Twin Otter measurements. Adjustments to predicted inorganic mass concentrations, based on predicted aerosol size distributions and the AMS transmission efficiency, are shown to be significant. Owing to recent shipping emission reductions, the dominant source of sulfate in the L.A. Basin may now be long-range transport. Sensitivity studies suggest that severely underestimated ammonia emissions, and not the exclusion of crustal species (Ca^{2+}, K^{+}, and Mg^{2+}), are the single largest contributor to measurement/model disagreement in the eastern part of the L.A. Basin. Despite overstated NO_x emissions, total nitrate concentrations are underpredicted, which suggests a missing source of HNO_3 and/or overprediction of deposition rates. Adding gas-phase NH_3 measurements and size-resolved measurements, up to 10 μm, of nitrate and various cations (e.g. Na^{+}, Ca^{2+}, K^{+}) to routine monitoring stations in the L.A. Basin would greatly facilitate interpreting day-to-day fluctuations in fine and coarse inorganic aerosol.

Citation: Ensberg, J. J., et al. (2013), Inorganic and black carbon aerosols in the Los Angeles Basin during CalNex, *J. Geophys. Res. Atmos.*, *118*, 1777–1803, doi:10.1029/2012JD018136.

All supporting information may be found in the online version of this article.

[1]Division of Chemistry and Chemical Engineering, California Institute of Technology, Pasadena, California, USA.
[2]Now at the Combustion Research Facility at Sandia National Laboratories, Livermore, California, USA.
[3]National Centre for Atmospheric Science, University of Manchester, Manchester, UK.
[4]School of Earth, Atmospheric and Environmental Sciences, University of Manchester, Manchester, UK.
[5]Cooperative Institute for Research in Environmental Sciences, University of Colorado Boulder, Boulder, Colorado, USA.
[6]Chemical Sciences Division, Earth System Research Laboratory, NOAA, Boulder, Colorado, USA.
[7]Now at the Department of Environmental Sciences University of California, Riverside, Riverside, California, USA.
[8]Planning and Technical Support Division, Air Resources Board, California Environmental Protection Agency, Sacramento, California, USA.
[9]Now at Harvard University, Cambridge, Massachusetts, USA.
[10]Department of Earth and Atmospheric Sciences, University of Houston, Houston, Texas, USA.
[11]Department of Chemistry and Biochemistry, University of Colorado, Boulder, Colorado, USA.
[12]Department of Chemistry, University of Toronto, Toronto, Ontario, Canada.
[13]Department of Atmospheric Sciences, University of California, Los Angeles, California, USA.
[14]Now at the Max Planck Institute for Chemistry in Mainz, Germany.
[15]Division of Engineering and Applied Science, California Institute of Technology, Pasadena, California, USA.

Corresponding author: J. H. Seinfeld, Division of Chemistry and Chemical Engineering, California Institute of Technology, Pasadena, California, USA. (seinfeld@caltech.edu)

2169-897X/13/2012JD018136

1. Introduction

[2] The Los Angeles mega-city has consistently experienced among the highest particulate matter levels in the United States and the highest ozone levels (http://www.stateoftheair.org/2012/city-rankings/most-polluted-cities.html). Several measurement campaigns have focused on characterizing particulate air quality in the Los Angeles Basin (e.g. *Appel et al*. [1982]; *Turpin and Huntzicker* [1991]; *Chow et al*. [1994]; *Watson et al*. [1994]; *Eldering et al*. [1994]; *Liu et al*. [2000]; *Hughes et al*. [2002]; *Pastor et al*. [2003]; *Croes and Fujita* [2003]; *Neuman et al*. [2003]; *Jacob et al*. [2010]; *Docherty et al*. [2011]), and in other urban areas, such as Pittsburgh, PA (Pittsburgh Air Quality Study, PAQS; e.g. *Wittig et al*. [2004]; *Cabada et al*. [2004]; *Modey et al*. [2004]; *Pekney et al*. [2006]; *Bein et al*. [2006]), Mexico City, Mexico (Mega-city Initiative: Local and Global Research Observations, MILAGRO; e.g. *Salcedo et al*. [2006]; *DeCarlo et al*. [2008]; *Querol et al*. [2008]; *Molina et al*. [2010]), Houston, Texas (2006 TexasAir Quality Study, TexAQS; e.g. *Parrish et al*. [2009]; *Nowak et al*. [2010]; *Washenfelder et al*. [2010]), and Beijing, China (Campaign of Air Quality Research in Beijing, CAREBEIJING; e.g. *van Pinxteren et al*. [2009]; *Yue et al*. [2009, 2010]; *Ianniello et al*. [2011]; *Zheng et al*. [2011]). Many studies have used data gathered during these field campaigns to evaluate the fidelity of three-dimensional atmospheric chemical transport models (CTMs) (e.g. *Sarwar and Bhave* [2007]; *Fountoukis and Nenes* [2007]; *Nolte et al*. [2008]; *Matsui et al*. [2009]; *Fountoukis et al*. [2009]; *McKeen et al*. [2009]; *Fast et al*. [2009]; *Foley et al*. [2010]; *Renner and Wolke* [2010]; *Zhang and Ying* [2010]; *Karydis et al*. [2010]; *Kelly et al*. [2010]; *Lee et al*. [2011]; *Huang et al*. [2011]; *Pfister et al*. [2011]).

[3] The California Research at the Nexus of Air Quality and Climate Change (CalNex) study was conducted during May–June 2010 to address both air quality and climate change through coordination and collaboration between several government agencies, such as the California Air Resources Board (CARB), the National Oceanic and Atmospheric Administration (NOAA), and academic institutions (www.esrl.noaa.gov/csd/calnex/). During CalNex, state-of-the-art airborne, ship-based, and ground-based measurements of atmospheric species, and of their transport over and off the coast of California, were conducted with the goal of understanding the impact of airborne pollutants on air quality and climate.

[4] The motivation for the present work is to evaluate the extent to which we understand the observed behavior of inorganic aerosols in the Los Angeles airshed, one of the world's most important urban areas from the point of view of air quality. The suite of ground-level and airborne measurements made during CalNex represent, by far, the most complete characterization of Los Angeles air quality yet carried out. Such a complex suite of measurements, gas and particle, surface and aloft, can only be placed in a unified context through the integration of chemistry and physics provided by a state-of-the-science atmospheric chemical transport model, driven by appropriate meteorology for the days of the experiment and operating on the emissions inventory of the region assembled by the relevant governmental agencies. In many respects, the current work can be seen as a parallel to the Mexico City MILAGRO study [*Molina et al*., 2010].

[5] To evaluate the extent to which predictions of a state-of-the-science CTM, driven by current emission inventories and resolved meteorological fields, agree with measured concentrations, we employ the Community Multiscale Air Quality (CMAQ) model version4.7.1 (http://www.cmaq-model.org/, *Foley et al*. [2010]) to simulate the three-dimensional distribution of aerosols and gases over Southern California during the CalNex field campaign. Predictions are compared to a suite of airborne and ground-based meteorological measurements, gas- and aerosol-phase inorganic measurements, and black carbon (BC) measurements over Southern California during the CalNex field campaign. Airborne measurements took place onboard the Center for Interdisciplinary Remotely-Piloted Aircraft Studies (CIRPAS) Navy Twin Otter aircraft (hereafter referred to as the Twin Otter) and the NOAA WP-3D (hereafter referred to as the P3) aircraft during May and June 2010. A Lagrangian particle dispersion model, FLEXPART (http://transport.nilu.no/flexpart, *Stohl et al*. [2005]), is used to track the origins of measured and predicted species in the Los Angeles Basin during CalNex by calculating back trajectories based on advection and turbulent mixing processes. Our goal is to identify the major sources of measurement/model disagreement for BC and various inorganic aerosol species and to suggest additional measures that address these sources of error. The organic component of the particulate matter will be addressed in a future study.

2. Model Description and Application

2.1. CMAQ

[6] In this study, we use CMAQ version 4.7.1 [*Foley et al*., 2010] on a domain that includes a large portion of Southern California as well as parts of Mexico (Figure 1), covering the area from (31.83°N, 121.43°W) to (35.69°N, 114.43°W) with 4 km by 4 km horizontal grid cells (102 x 156 grid points). Simulations cover the time period of May 2010. All simulations include a minimum spin-up period of four days to mitigate the influence of initial conditions, except for the P3 flight during 4 May 2012 which included only three days of spin up due to lack of MM5 meteorology for 30 April 2010. The meteorological fields used to drive the model were generated by the 5th generation Penn State/National Center for Atmospheric Research Meso-scale Model (MM5 version 3.7.4; *Grell et al*. [1995]). Three nested grids, with horizontal resolutions of 36, 12, and 4 km, were used to generate meteorological fields at the desired resolution (Figure S1). Nesting is the process by which a model simulation is run over a certain domain (the parent domain) at a given resolution. From the predicted concentrations within the parent domain, boundary conditions are extracted and used to drive a separate finer-resolution model simulation that is run over a portion of the parent domain (the nested domain). The MM5 model was initialized from NARR analysis data (http://nomads.ncdc.noaa.gov/data/narr/) with analysis nudging option, but observational nudging was not used. The 36 km and 12 km grids were first run together, via two-way nesting, using the Grell cumulus, simple ice microphysics, NOAH soil scheme, MRF PBL, and RRTM radiation options. The 4 km grid was then run, via one-way nesting, using boundary conditions derived from the 12 km grid with all options identical to the coarse domain simulations, except that the cumulus parameterization was turned off since the sufficiently fine horizontal

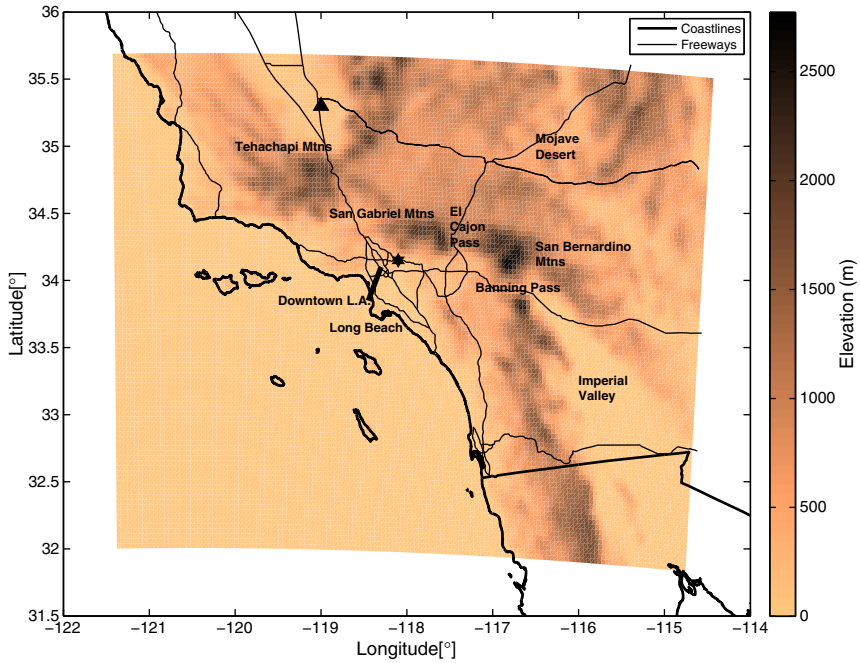

Figure 1. CMAQ modeling domain (colored area) used for simulations during the CalNex Field Campaign. The domain covers the area from (31.83°N, 121.43°W) to (35.69°N, 114.43°W) with 4 km x 4 km horizontal grid cells (102 x 156 grid points). The star represents the Pasadena ground site and the triangle represents Bakersfield.

resolution of the 4 km grid is expected to capture the smaller cloud scale atmospheric motions. CMAQ-compatible meteorological fields were then generated by processing MM5 output using the Meteorology-Chemistry Interface Program (MCIP) version 3.6 [*Otte and Pleim*, 2010]. Vertically, the meteorological fields extend from the surface to 100 mb (∼18 km above sea level) using 30 layers. This vertical resolution is typical for regional-scale and meso-scale modeling studies such as this. For instance, *Kelly et al.* [2010] configured CMAQ to use 30 vertical layers for the coast of Florida. Similarly, *Foley et al.* [2010] tested CMAQ4.7 over the eastern United States using 12, 24, and 34 vertical layers. In the present study, there are 11 layers in the lowest 1000 m, and the surface layer is ∼30 m deep.

[7] The emission inventory used in this study is a modified version of the day-specific ARCTAS-CARB inventory from June 2008. The modification consists of averaging June emissions to produce emissions for one representative week-day and one representative weekend-day for use during May 2010. In so doing, it is implicitly assumed that emissions did not change appreciably from 2008 to 2010. This assumption may be in question due to the recent emissions control programs, such as the diesel truck rules and ocean going vessel (OGV) fuel regulations (http://www.arb.ca.gov/msprog/operators.htm). As a result, emissions of BC and sulfur containing compounds may have decreased significantly from 2008 to 2010 [*Dallmann et al.*, 2011; *Lack et al.*, 2011]. The CARB recognizes this limitation and is working toward releasing a newer version of the emission inventory. Daily total emission rates for each species are given in Tables S4 and S5, and the emission inventory used in this study is available from the authors upon request. The limitations of the current CARB inventory are expected to impact agreement between observations and predictions of anthropogenic BC and sulfur containing compounds, but not sea-salt emissions of SO_4^{2-} which are modeled interactively in CMAQ [*Gong*, 2003; *Sarwar and Bhave*, 2007; *Kelly et al.*, 2010]. All meteorological fields and gridded emission inventories were prepared and provided by CARB.

[8] Gas-phase predictions are based on a modified version of the Statewide Air Pollution Research Center (SAPRC) chemical mechanism (version SAPRC07TC, *Carter* [2010]) implemented in CMAQ with the Rosenbrock numerical solver. The main modification consists of using an updated isoprene photooxidation mechanism based on *Paulot et al.* [2009a, 2009b]. Atmospheric mass distributions of particulate matter by size are represented in CMAQ as the superposition of three log-normal distributions, referred to as modes. These are the Aitken mode (typical D_p range is 20 nm to 90 nm), the accumulation mode (typical D_p range is 90 nm to 1-2.5 μm), and the coarse aerosol mode (typical D_p range is 1-2.5 to 10 μm) [*Binkowski and Roselle*, 2003]. Each mode is defined by its geometric standard deviation, geometric mean diameter, and the magnitude of mass within the mode. All particles are assumed to be spherical and each mode is assumed to be internally mixed chemically. Aerosol processes such as evaporation, condensation, coagulation, nucleation, advection, and wet and dry deposition affect the total number of particles, total surface area, and total mass within each mode. The majority of primary $PM_{2.5}$ emissions (99.9% by mass), including BC, are assigned to the accumulation mode, and a small fraction (0.1% by mass) is assigned to the Aitken mode according to section 1.3 of *Binkowski and Roselle* [2003].

[9] The thermodynamic model ISORROPIA-II [*Fountoukis and Nenes*, 2007] is used in CMAQ to compute the thermodynamic equilibrium of the NH_4^+-Na^+-SO_4^{2-}-NO_3^--Cl^--H_2O aerosol system. The assumption of thermodynamic equilibrium between fine inorganic particulate nitrate and ammonium with gas-phase nitric acid and ammonia is commonly invoked in atmospheric CTMs. The validity of this assumption for fine particles (D_p typically < 2.5 μm) was confirmed on the basis of data obtained during the 1999 Atlanta Supersite Experiment [*Zhang et al*., 2002]. *Karydis et al*. [2010] used the PMCAMx model with ISORROPIA-II to model inorganic aerosol measured during the Mexico City MILAGRO campaign. They concluded that explicitly treating mass transfer to and from coarse aerosol as a dynamic process is essential for capturing the competition between small and large particles for condensible inorganic vapors. To account for this competition, CMAQ partitions mass between the gas and aerosol phases according to the hybrid method [*Capaldo et al*., 2000], in which instantaneous equilibrium is assumed between the gas and aerosol phases in the two fine modes, and dynamic mass transfer governs the coarse aerosol mode. Since ISORROPIA-II is capable of simulating aerosol systems that include K^+-Ca^{2+}-Mg^{2+}, we conduct an additional sensitivity simulation on the impact of dust emissions and crustal species on inorganic aerosol concentrations in the L.A. Basin.

2.2. GEOS-Chem

[10] Dynamic chemical boundary conditions (1-h temporal resolution) used in the CMAQ simulations were generated from the GEOS-Chem global chemical transport model (version 9-01-01, http://acmg.seas.harvard.edu/geos/) via one-way nesting. GEOS-Chem was used to simulate global gas- and aerosol-phase concentrations at 2° latitude x 2.5° longitude horizontal resolution, with 47 vertical levels. Boundary conditions were extracted from the global simulation and used to drive a nested GEOS-Chem simulation over North America at 0.5° latitude x 0.667° longitude horizontal resolution, with 47 vertical levels. Finally, CMAQ-consistent boundary conditions were then extracted from the nested GEOS-Chem simulations for the domain shown in Figure 1. All three domains are shown on a single map in Figure S2. The coarse GEOS-Chem parent grid simulation spin-up period was 1 year, and the spin-up period for the nested GEOS-Chem grid simulation was 4 months (Jan-Apr 2010). Goddard Earth Observing System (GEOS-5) assimilated meteorological data from the NASA Global Modeling and Assimilation Office (GMAO) were used for all GEOS-Chem model simulations, which included ozone-NO_x-hydrocarbon chemistry [*Bey et al*., 2001] coupled with sulfate-nitrate-ammonium aerosol chemistry [*Park et al*., 2004]. Outside North America, global emissions used in the coarse simulations are from the Emissions Database for Global Atmospheric Research (EDGAR) inventory [*Olivier and Berdowski*, 2001]. Anthropogenic emissions data for the United States, used in GEOS-Chem, were from the EPA National Emissions Inventory (NEI) 2005, scaled to the simulation period according to trends in the EPA Acid Rain Program (http://camddataandmaps.epa.gov/gdm/) and the NEI Air Pollutant Emissions Trends Data (http://www.epa.gov/ttn/chief/trends/). The nested GEOS-Chem simulation also includes aircraft, biofuel and natural emissions of inorganic aerosol precursors, as described by *Park et al*. [2004].

[11] Since the nested GEOS-Chem horizontal grid resolution of 0.5° latitude x 0.667° longitude (~55 km x ~60 km at latitude 33°N) is considerably coarser than the 4 km x 4 km resolution of CMAQ, and the domain shown in Figure 1 is relatively small compared to the North American continent, the potential double-counting of species in the L.A. Basin was taken into consideration. Coarse resolution acts to smooth concentration gradients via dilution, thereby reducing peak values within the region and increasing species concentrations at the boundaries. These species can then partially reenter the L.A. Basin as boundary conditions, while simultaneously being emitted within the L.A. Basin via the ARCTAS-CARB emission inventory, which is physically unrealistic. However, it is possible for species emitted in the L.A. Basin to be transported outside the domain (Figure 1), and then reenter via recirculation. To determine the impacts of both of these potential issues, additional sensitivity simulations have been conducted with CMAQ using two sets of boundary conditions: (1) one set is derived from a nested GEOS-Chem simulation over North America that includes emissions in the L.A. Basin, and (2) one set is derived from the same nested GEOS-Chem simulation over North America with emissions in the domain shown in Figure 1 set to zero (the latter set was used in the results to be presented). The results (not shown) indicate that the impact of turning off emissions in the L.A. Basin in the nested GEOS-Chem simulation has virtually no impact on black carbon concentrations, and only a very slight impact on the boundary inflow of sulfate. Therefore recirculation and the potential double-counting of species are not issues in the current model configuration, although this may not be true for modeling configurations with different domain sizes and different grid-cell sizes, or if there are significant emissions sources near the boundaries of the nested domain.

2.3. FLEXPART

[12] To trace the origins of measured and predicted species during CalNex, a modified version of the FLEXPART Lagrangian particle dispersion model [*Stohl et al*., 2005] is used to calculate back trajectories of air masses. FLEXPART has been used extensively to quantify the impacts of meteorological processes on pollution transport (e.g., *de Foy et al*. [2006]; *Palau et al*. [2006]; *Ding et al*. [2009]; *Brioude et al*. [2009]). A detailed description of the FLEXPART model used in this study can be found in the Supplementary Material.

3. Observations

3.1. Pasadena Ground-Site Data

[13] Planetary boundary layer (PBL) heights were measured at the Pasadena ground site with a Vaisala Ceilometer CL31, which uses the minimum-gradient method to determine aerosol backscatter profiles [*Emeis and Schafer*, 2006; *Schafer et al*., 2004]. Observed PBL heights are compared to predicted PBL heights in Figure 2. Previous studies have shown overall agreement between this technique as compared to radiosonde and sonic detection and ranging estimates of PBL height [*Haman*, 2011; *van der Kamp et al*., 2010; *Martucci et al*., 2007; *Münkel et al*., 2006]. For this study, the average PBL height uncertainty and the minimum detection limit are ±5m and ~80 m, respectively. A detailed description of the instruments and settings used in this study can be found in *Haman* [2011].

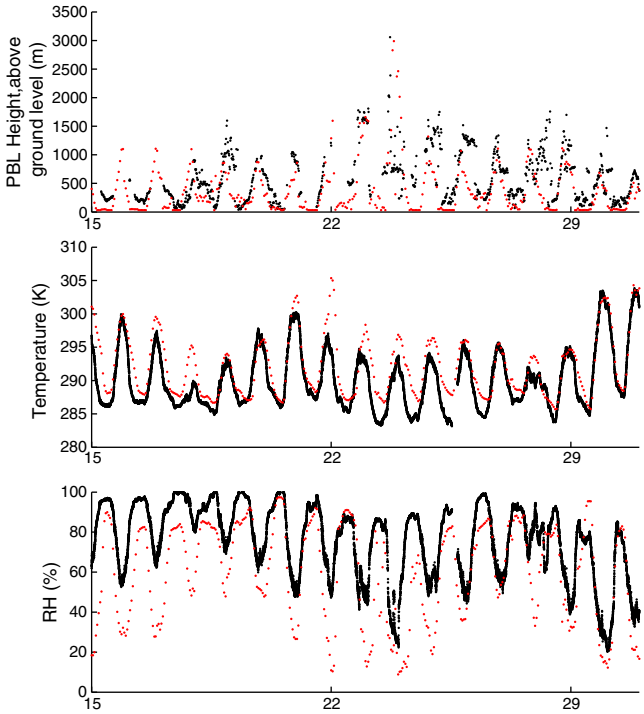

Figure 2. Observed (black) and predicted (red) planetary boundary layer (PBL) heights, temperature, and relative humidity (RH) at the Pasadena ground site from 15 May–31 May 2010.

[14] Refractory black carbon (BC) aerosol mass was measured at the Pasadena ground-site with a Droplet Measurement Technologies (DMT, Boulder, CO, USA) Single Particle Soot Photometer (SP2). Briefly, the SP2 detects refractory BC mass by measuring the incandescence signal emitted from single BC-containing particles heated to their boiling point when passing through an intense Nd:YAG laser beam (λ =1064 nm). BC volume-equivalent diameter (VED) is calculated from the detected mass assuming a spherical particle with density of 1.8 g cm^{-3} [*Bond and Bergstrom*, 2006]. The SP2 incandescence channels were calibrated in the same way as described in Section 2 of the Supplemental Material to *McMeeking et al.* [2010], with the main difference being that Alfa Aesar glassy carbon spheres were used instead of Aquadag. The data have been corrected for mass above and below the detection limit of the instrument by fitting a log-normal distribution to the primary mode in the BC mass distribution and another log-normal distribution to the residual of this fit (i.e. a secondary mode). The two fits were then added together, and the fraction of the fits above and below the SP2 detection limit were calculated as 8.0% of BC mass below the detection limit and 1.9% above. The measured BC mass concentrations have been divided by (1- 0.099). Based on *Shiraiwa et al.* [2008] and *Schwarz et al.* [2008b], the uncertainty in the determination of the mass of a single BC particle measured at the Pasadena ground site is estimated to be ~30%. All BC measurements from the Pasadena ground site are shown in Figure 3.

[15] Inorganic aerosol measurements were made by the University of Colorado-Boulder Aerodyne high-resolution time-of-flight aerosol mass spectrometer (Aerodyne HR-ToF-AMS, Aerodyne Research, Inc., Billerica, MA USA, [*DeCarlo et al.*, 2008]) at the CalNex Pasadena ground site. The inlet is designed to transmit particles with vacuum-aerodynamic diameters (D_{va}) of 60 to 600 nm with unit transmission efficiency, although particles with D_{va} above 600 nm are also detected [*Canagaratna et al.*, 2007; *DeCarlo et al.*, 2004]. A composition-dependent collection efficiency (CE) was applied to the AMS data based on

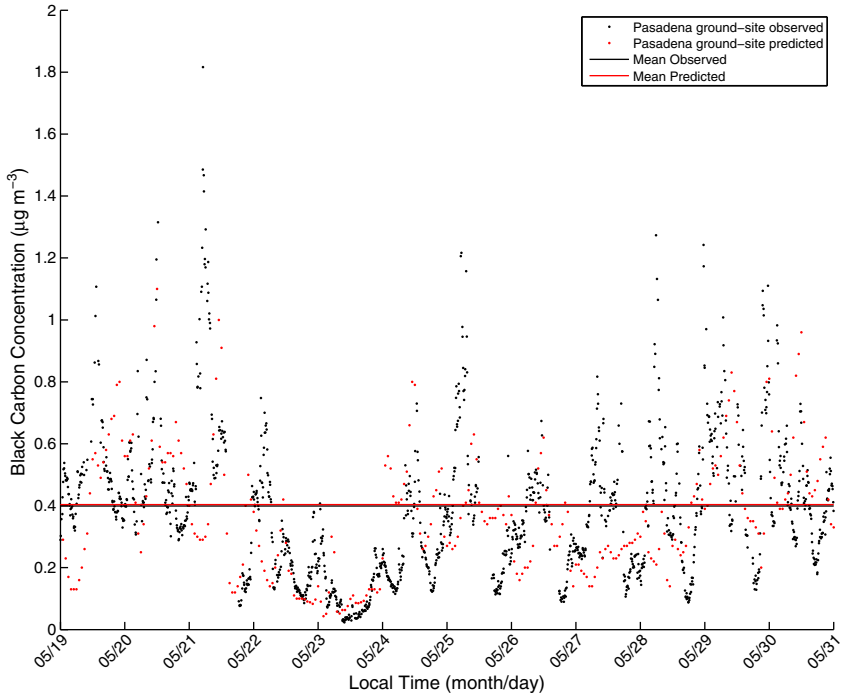

Figure 3. Measured (black dots) and predicted (red dots) BC concentrations at the Pasadena ground site from 19 May – 31 May 2010.

recent work [*Middlebrook et al*., 2012]. The composition based method for collection efficiency addresses the issue of particle bounce in the AMS and that particle bounce is a function of particle phase. The technique presented by *Middlebrook et al*. [2012] encompasses the four main factors influencing particle phase: relative humidity in the sampling line, acidity/neutralization of the sulfate content, ammonium nitrate content, and organic liquid content. For this data set, there were several instances where ammonium nitrate dominated the aerosol mass, and as shown in Figure 3 in *Middlebrook et al*. [2012], when the ammonium nitrate fraction exceeds 0.4, the CE for the aerosol increases from 0.45 to 1. Using a constant CE value during these periods would cause an overprediction of aerosol mass. The ground-site AMS measurements are reported as 5-min averages and have an uncertainty <30%. NH_3 was measured at 1 Hz by quantum cascade tunable infrared laser differential absorption spectroscopy (QC-TILDAS from Aerodyne Inc.) with an overall uncertainty during the CalNex campaign of 10% + 0.42 ppbv. [*Ellis et al*., 2010]. HNO_3 measurements were made with the acetate ion CIMS described by *Roberts et al*. [2010]. Data were acquired every 10 seconds, and were averaged to one minute. The calibrations were performed with permeation tubes calibrated as described by [*Neuman et al*., 2002]. The time constant for transmission of HNO_3 through the inlet was found to be several minutes. The overall uncertainty of the HNO_3 measurement was 34% + 0.05 ppbv. SO_2 mixing ratios were measured at the Pasadena site with a commercial pulsed fluorescence detector (Model 43i-TL, Thermo Electron Corp) operated as described in *Luke* [1997]. All inorganic species measurements from the Pasadena ground site are shown in Figure 4. Hourly measurements of NO_x and SO_2 at three ground sites in the L.A. Basin are also reported by the CARB ground network (http://www.arb.ca.gov/aqmis2/aqmis2.php) and shown in Figure 5.

3.2. CIRPAS Twin Otter

[16] BC aerosol mass was measured onboard the Twin Otter aircraft with a Droplet Measurement Technologies (DMT, Boulder, CO, USA) Single Particle Soot Photometer (SP2). The major findings from this SP2 during CalNex, including calibration of the instrument, are detailed elsewhere

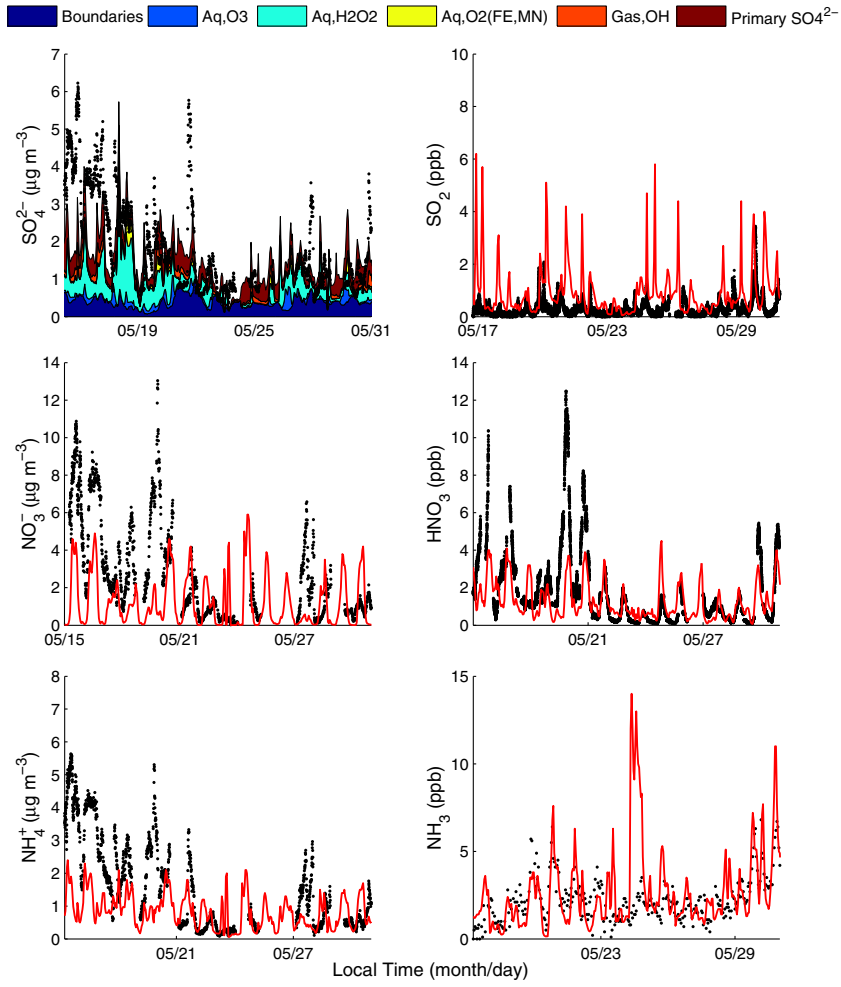

Figure 4. Observed (black) and predicted (red) particulate sulfate, nitrate, ammonium, sulfur dioxide, nitric acid, and ammonia concentrations from the CalNex Pasadena ground site. In the legend, "Boundaries" refers to sulfate attributable to boundary conditions, "(Aq,Gas),OX" refers to secondary sulfate produced by aqueous-phase (Aq) or gas-phase (Gas) oxidation of SO_2 by oxidant OX. "Primary SO_4^{2-}" refers to sulfate emitted within the basin.

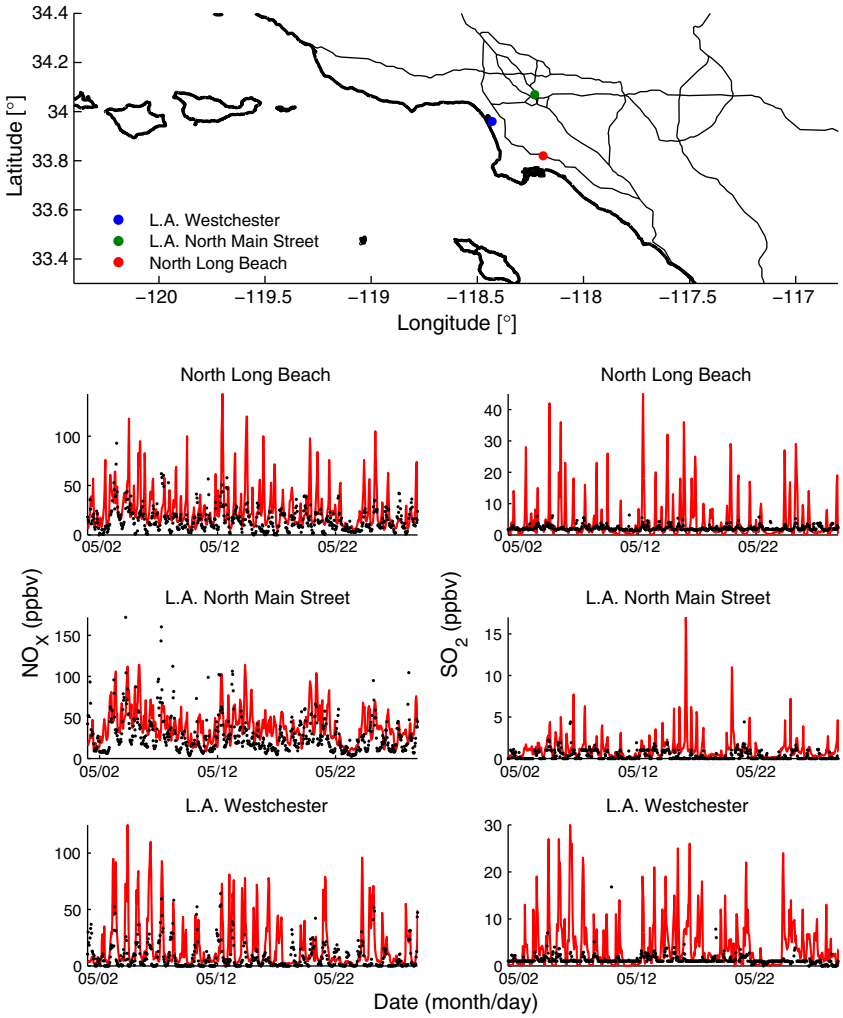

Figure 5. Measured (black) and predicted (red) NO_x and SO_2 mixing ratios for May 2010 at three locations in the Los Angeles Basin. Gaseous measurements were taken from the Air Quality and Meteorological Information System (AQMIS, http://www.arb.ca.gov/aqmis2/aqmis2.php).

[*Metcalf et al*., 2012]. In *Metcalf et al*. [2012], 1-min average data are reported, but in this study, we have re-sampled the dataset at 1 Hz to take advantage of the highest time-resolution available. To account for the BC mass outside the SP2 detection range, a single log-normal function is fit to each 1-s histogram of single-particle BC mass between 0.48 and 290 fg (50-675 nm VED, assuming a spherical particle density of 1.8 g cm^{-3}), and integrated to give bulk BC mass concentrations. Unlike the SP2 measurements at the Pasadena ground site, a single log-normal mode is sufficient to adjust the measured BC size distributions for mass above and below the Twin Otter SP2 detection limits [*Metcalf et al*., 2012]. As discussed in *Metcalf et al*. [2012], this adjustment increases bulk BC mass concentrations by 15–20%. Based on the calibration standards available, uncertainty in single-particle BC mass determination and bulk mass concentrations is estimated to be ~40%.

[17] Non-refractory particle mass and composition measurements were made by an Aerodyne compact time-of-flight aerosol mass spectrometer (C-ToF-AMS, Aerodyne Research, Inc., Billerica, MA USA) [*Drewnick et al*., 2005; *Murphy et al*., 2009]. The AMS onboard the Twin Otter measures sub-micron, non-refractory, size-resolved aerosol composition. The inlet and collection efficiency of the AMS onboard the Twin Otter were similar to those of the AMS at the Pasadena ground site. In an effort to measure aerosol mass distributions, the AMS onboard the Twin Otter was periodically run in particle-time-of-flight (PToF) mode. Due to relatively low aerosol loadings, the signal-to-noise ratio was not of sufficient quality for a meaningful comparison to size distributions predicted by CMAQ. Instead, we focus on bulk particulate ammonium (NH_4^+), particulate nitrate (NO_3^-), and particulate sulfate (SO_4^{2-}) mass concentrations reported as 10-s averages. We note that due to the attempted size-resolved measurements, narrow plumes may have been missed by the AMS onboard the Twin Otter.

[18] All Twin Otter measurements reported here are from instruments inside an unpressurized cabin. All instruments sampled downstream of a two-stage diffusion inlet with a transmission efficiency near unity for particle diameters up to about 3.5 μm [*Hegg et al*., 2005]. Sampling lines inside the cabin are kept reasonably uniform to all instruments, so further corrections for diffusional losses in these lines have not been made. The Twin Otter conducted 18 research

flights from Ontario, CA between 4 May and 28 May 2010 during CalNex. The AMS was onboard during 8 of the flights, three of which were to San Joaquin Valley, which is outside the domain shown in Figure 1. Therefore, this analysis makes use of 5 Twin Otter flights during which inorganic aerosol concentrations were measured within the L.A. Basin.

3.3. NOAA P3

[19] The P3 aircraft conducted 18 research flights from Ontario, CA between 4 May and 20 June 2010 during CalNex 2010 (esrl.noaa.gov/csd/calnex/). This study uses daytime measurements from 5 P3 flights that focused on sampling L. A. Basin emissions and the resulting photochemical products. NH_3, HNO_3, NH_4^+, NO_3^-, and SO_4^{2-}, and various meteorological parameters were measured onboard the P3 aircraft. NH_3 was measured at 1 Hz (equivalent to 100 m spatial resolution) by chemical ionization mass spectrometry (CIMS) with typical uncertainties of (30% + 0.2 ppbv) and a 1σ imprecision of 0.08 ppbv [*Nowak et al*., 2010]. HNO_3 was measured at 1 Hz by a separate CIMS instrument with an uncertainty of (15% + 0.040 ppbv) and a 1σ imprecision of 0.012 ppbv [*Neuman et al*., 2012]. CO measurements were made by a vacuum ultraviolet fluorescence instrument with ±5% uncertainty and 1 ppbv imprecision [*Holloway et al*., 2000]. SO_4^{2-}, NH_4^+, and NO_3^- were measured from a pressure-controlled region downstream of a low turbulence inlet using a compact time-of-flight aerosol mass spectrometer (Aerodyne, Billerica, Massachusetts) [*Bahreini et al*., 2009]. The AMS data are reported as 10-s averages with 2σ uncertainty (1-σ imprecision) of 34% (0.06 μg m^{-3}), 34% (0.01 μg m^{-3}), and 36% (0.01 μg m^{-3}) for ammonium, nitrate, and sulfate, respectively. BC measurements in the size range of 95-720 nm VED (still assuming a BC void-free density of 1.8 g cm^{-3}) were made by an SP2 similar to that used onboard the Twin Otter [*Schwarz et al*., 2006]. As with the SP2 measurements onboard the Twin Otter, a single log-normal function is sufficient to account for mass above and below the P3 SP2 detection limits, and this adjustment increases bulk BC mass concentrations by 10–25%. As described in detail in *Metcalf et al*. [2012], due to differences in calibration, measurements from the SP2 onboard the Twin Otter are potentially biased low by ∼12%, as compared to those from the SP2 onboard the P3 (e.g. if the P3 measurement is 1 μg m^{-3}, the Twin Otter measurement would be 0.88 μg m^{-3}).

[20] The AMSs used in this study, both ground-based and airborne, measured only particles with vacuum aerodynamic diameters between 60 nm and 600 nm diameter with 100% efficiency. Particles with aerodynamic diameters above 600 nm were also measured, but with reduced collection efficiency. However, since the predicted Aitken, accumulation, and coarse aerosol modes are expressed in CMAQ in terms of log-normal functions, each mode is defined for particle diameters ranging from zero to infinity. Therefore, all aerosol predictions are adjusted to match the transmission efficiency of the AMS based on the following piece-wise defined transmission function:

- 0% transmission below D_{va} = 40 nm;
- linear increase in transmission vs ln(D_{va}), from 0% at D_{va} = 40 nm to 100% at D_{va} = 100 nm;
- 100% transmission from D_{va} = 100 nm up to D_{va} = 550 nm;
- linear decrease in transmission vs ln(D_{va}), from 100% at D_{va} = 550 nm to 0% at D_{va} = 2 μm.
- 0% transmission above D_{va} = 2 μm;

[21] This transmission function is an average of the transmission curves used in several AMS studies as described in *Knote et al*. [2011] and references therein, and is applied to all inorganic aerosol predictions (CMAQ) that are compared to AMS measurements from the Pasadena site, the Twin Otter aircraft, and the P3 aircraft. We note that due to variation between specific aerodynamic lenses in different instruments, the exact transmission efficiencies of the AMS at the Pasadena site, onboard the Twin Otter, and onboard the P3 will be slightly different than the one used in this study. Appendix B presents the equations used to modify CMAQ predictions based on the AMS transmission window and efficiencies, and a derivation of these equations is given in the Supplemental Material. Measured BC concentrations from all platforms, adjusted for mass above and below the SP2 detection limits, are compared directly to the unmodified predicted BC concentrations in all results to be presented.

4. Results and Discussion

[22] The Aerosol Modeling Testbed analysis toolkit [*Fast et al*., 2011] was used to map three-dimensional CMAQ meteorological parameters, predicted gas-phase concentrations, and predicted aerosol-phase concentrations onto each flight path (as well as for various ground sites). The temporal resolution of the CARB emission inventory and MM5 meteorology is 1 h. In this work, CMAQ predicted species concentration fields, averaged over the previous hour, are compared to observations according to observational time-stamps (i.e. observational points with time-stamps of 12:20 and 12:40 would both be compared to predictions averaged between the hours of 12:00-13:00). The discrepancy between measured and simulated species concentration fields and meteorological parameters is quantitatively assessed using the following four statistical metrics:

$$ME = \frac{1}{N}\sum_{i=1}^{N}|P_i - M_i| \text{(mean error)} \quad (1)$$

$$MB = \frac{1}{N}\sum_{i=1}^{N}(P_i - M_i) \text{(mean bias)} \quad (2)$$

$$NME = \frac{\sum_{i=1}^{N}|P_i - M_i|}{\sum_{i=1}^{N}M_i} \text{(normalized mean error)} \quad (3)$$

$$NMB = \frac{\sum_{i=1}^{N}(P_i - M_i)}{\sum_{i=1}^{N}M_i} \text{(normalized mean bias)} \quad (4)$$

where N, P, and M stand for the number of data points, predicted quantity, and measured quantity, respectively.

4.1. Meteorological Variables

4.1.1. Ground Site

[23] Observed and predicted temperature, relative humidity (RH), and planetary boundary layer (PBL) height from the Pasadena ground site are shown in Figure 2 and statistical metrics are given in Table 1. Overall, the agreement

between observed and predicted PBL height in Pasadena has a 15-day average bias of -80 m (-9%). Agreement between observed and predicted temperature has a 15-day average bias of 1.06°C. The agreement between observed and predicted RH has a 15-day average bias of -10.3%. The discrepancies in RH are most likely a combination of underpredicted water vapor mixing ratios and of the exponential dependence of saturation-vapor pressure on errors in temperature (1°C temperature error leads to approximately 5% RH error). Additional ground-site comparisons of predicted and observed meteorology are given in the Supplemental Material. The results show that temperature and RH are consistently overpredicted and underpredicted, respectively, during the first week of May, with much better agreement during the last three weeks. Predicted wind speeds and wind directions agree to within 2 m/s and 60°, respectively, at all surface sites.

Table 1. Statistical Metrics Based on Measurements and Predictions at the Pasadena Ground Site During May 2010

Parameter	N	ME	MB	NME	NMB
PBL Height (m)	1179	129	-80	0.14	-0.09
Temperature (k)	24697	1.88	1.06		
RH (%)	24697	11.6	-10.3		
BC ($\mu g\ m^{-3}$)	3918	0.19	0.03	0.48	0.07
SO_4^{2-} ($\mu g\ m^{-3}$)	1860	0.93	-0.36	0.44	-0.17
NO_3^- ($\mu g\ m^{-3}$)	1860	2.15	-1.50	0.72	-0.50
NH_4^+ ($\mu g\ m^{-3}$)	1860	1.07	-0.76	0.35	-0.25
SO_2 (ppbv)	22491	0.72	0.64	2.50	2.01
HNO_3 (ppbv)	22761	0.98	-0.38	0.85	-0.38
NH_3 (ppbv)	366	1.51	0.45	0.74	0.22

ME = Mean Error, MB = Mean Bias, NME = Normalized Mean Error, NMB = Normalized Mean Bias. N is the number of data points collected during May 2010.

4.1.2. Twin Otter and P3

[24] The Twin Otter and P3 flight paths and altitudes are shown in Figures 6–11 and Appendix A Figures A1, A2, A3, A4. Temperature and relative humidity (RH) measurements from the Twin Otter and P3 flights are compared to

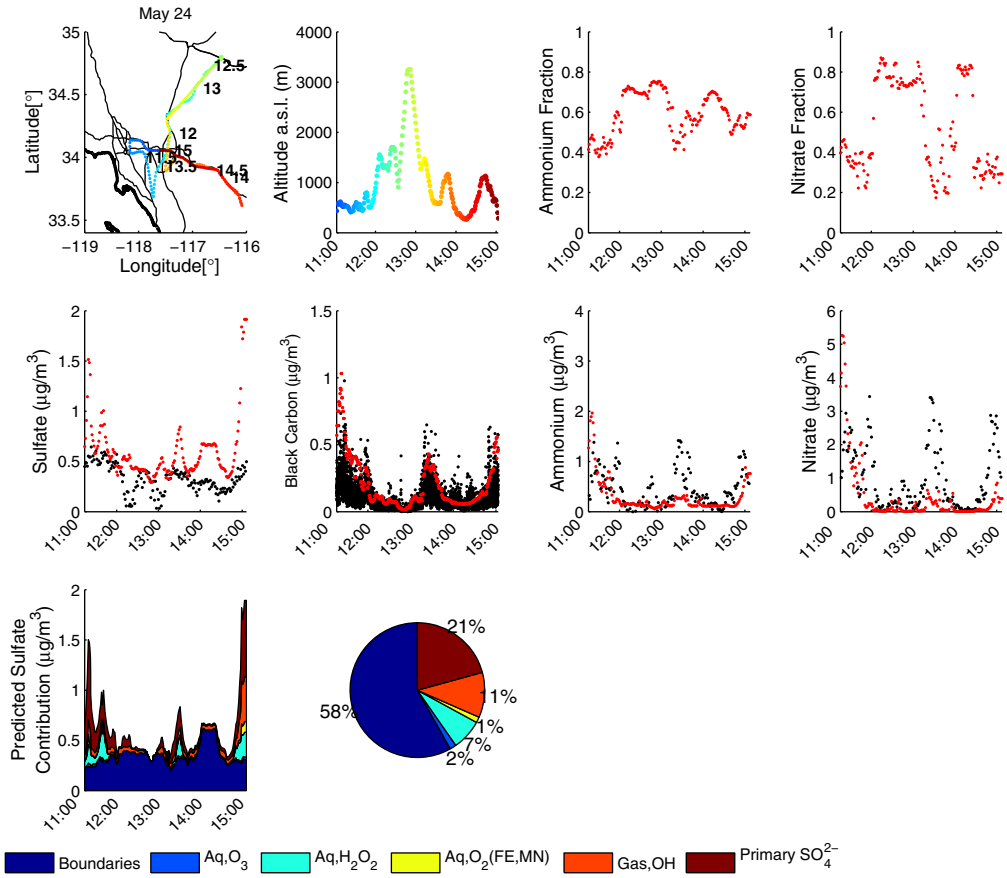

Figure 6. From left to right and top to bottom: Twin Otter aircraft flight path for May 24, Twin Otter altitudes (with respect to sea level) with the flight track and altitude trace are colored by the time (Pacific Standard Time) of day and time-stamps printed along each flight path in 30 min increments, Fraction of predicted particulate ammonium within the AMS transmission window, Fraction of predicted particulate nitrate within the AMS transmission window, predicted (red) and observed (black) sulfate concentrations, predicted (red) and observed (black) black carbon concentrations, predicted (red) and observed (black) nitrate concentrations, predicted (red) and observed (black) ammonium concentrations, predicted sulfate source apportionment, Pie chart indicating the relative contribution from routes to sulfate averaged over a given flight. In the bottom legend, "Boundaries" refers to sulfate attributable to boundary conditions, "(Aq,Gas),OX" refers to secondary sulfate produced by aqueous-phase (Aq) or gas-phase (Gas) oxidation of SO_2 by oxidant OX. "Primary SO_4^{2-}" refers to sulfate emitted within the basin.

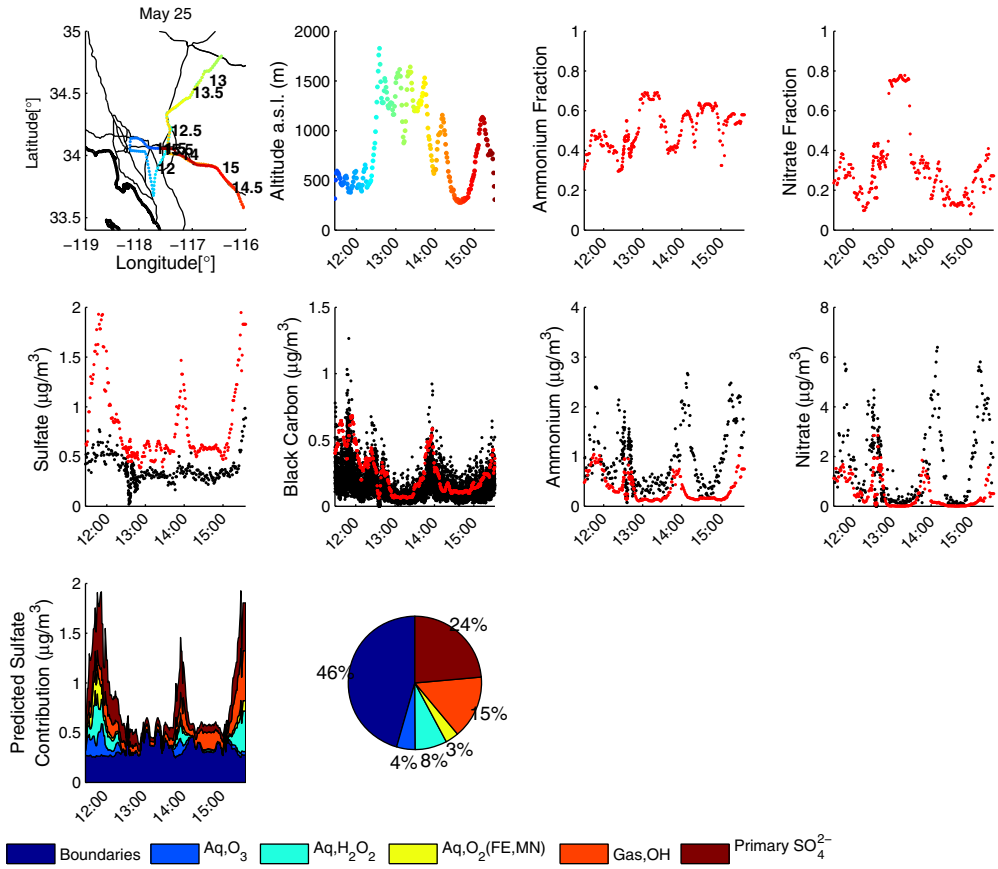

Figure 7. Same as Figure 6, but for the Twin Otter May 25 flight.

MM5 predictions in Table 2. Observed and predicted temperatures (averaged over each flight) typically agree to within 4°C, while observed and predicted RH (averaged over each flight) typically agree to within 15%. *Zhang et al.* [2006] evaluated MM5 meteorology coupled with CMAQ against measurements taken during the Southern Oxidants Study, and found similar levels of agreement between predicted and observed temperature and RH. In the present study, the largest disagreement occurred during the 21 May Twin Otter flight and the 14 May P3 flight, during which predicted RH was biased low by 26.6% and 22.1%, respectively. Wind speed and wind direction measurements onboard the Twin Otter and the P3 are shown in Table 3. Predicted and observed wind speeds generally agree to within ~50% when averaged over each flight. Although the mean discrepancy between predicted and observed wind direction ranges between 22-65°, the average predicted and observed wind direction is that of the daytime southwesterly sea breeze which advects emissions towards the north and northeast, exiting the Basin through passes in the San Gabriel and San Bernardino mountain ranges [*Lu and Turco*, 1995]. However, it is difficult to quantify errors in species concentrations attributable to discrepancies between measured and observed wind vectors.

4.2. Black Carbon

4.2.1. Pasadena Ground Site

[25] Measured and predicted BC concentrations at the Pasadena ground site are shown in Figure 3. The overall agreement between predicted and observed BC concentrations is very good, with a CalNex-average NME and NMB of 47.8% and 6.6%, respectively (Table 1). This NME of 47.8% is slightly higher than the measurement error inherent to the SP2 (~30–40%) owing mostly to large missing peaks in predicted BC on specific days (e.g. 27 and 28 May). Because predicted BC is chemically inert, the Pasadena ground-site is fixed, and all weekday emissions are assumed to be identical, day-to-day variations in BC predictions at the Pasadena ground site can only be caused by variations in the predicted meteorological fields (e.g. wind fields). For instance, May 20 and May 27 were both Thursdays. However, the 1-h average BC predictions on 27 May did not get above 0.4 μg^{-3}, while BC predictions on 20 May were up to 1.1 μg^{-3}. Since the predicted PBL heights on these days were comparable (Figure 2), variation in the predicted wind fields is the primary cause of the day-to-day variation in predicted BC concentrations. Therefore, if the differences between the predicted and observed wind fields on any given day are comparable to the day-to-day differences in the predicted wind fields, large errors in BC predictions may occur at any given point (e.g. Pasadena ground site). However, the overall agreement between predicted and observed BC at the Pasadena ground site (NMB = 6.6%) suggests that on average, both wind fields and upwind BC sources are represented well by CMAQ.

4.2.2. Twin Otter and P3

[26] Measured and predicted BC concentrations from the Twin Otter flights and the P3 flights during May 2010 are shown in Figures 6–11 and Figures A1, A2, A3, A4. The illusory differences in noise levels of the Twin Otter BC

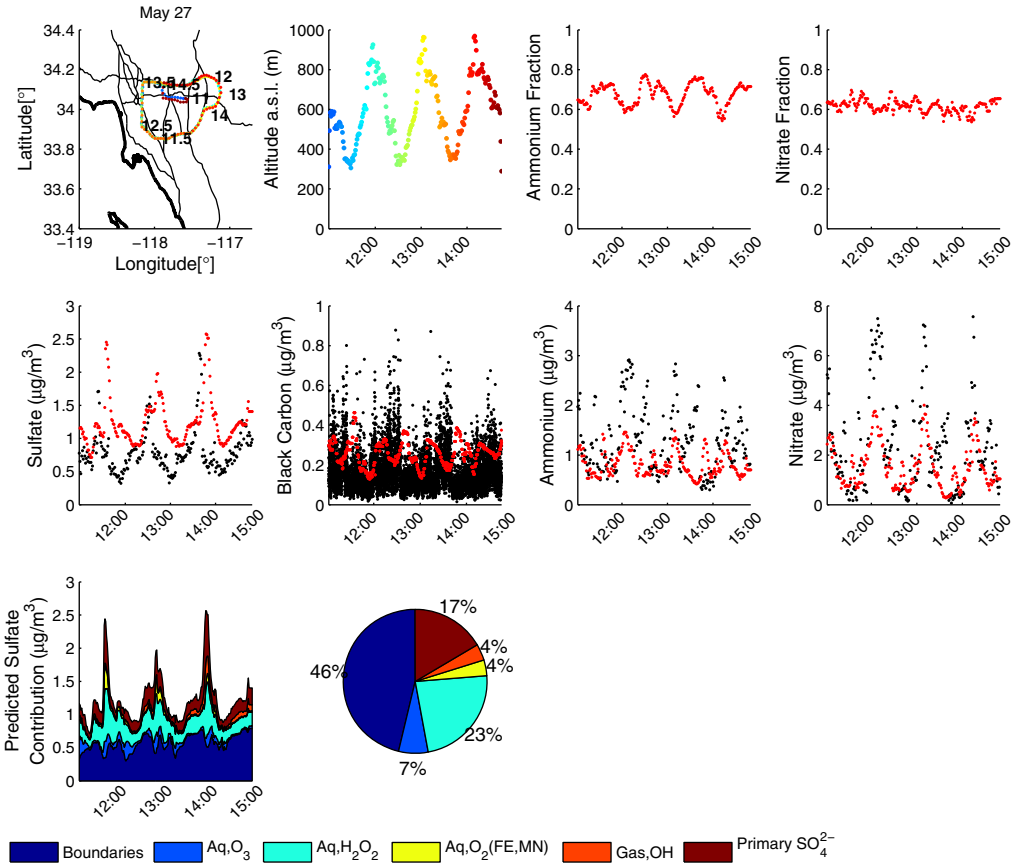

Figure 8. Same as Figure 6, but for the Twin Otter May 27 flight.

measurements and the P3 BC measurements exist because (1) the P3 aircraft transitioned between high and low altitudes many times during each flight, which creates the appearance of less noise due to very low BC concentrations at high altitudes, and (2) the average P3 flight was roughly 1.5 times longer than the average Twin Otter flight, but the x-axes in all time-series plots are the same length. Therefore, the P3 time-series are more compressed and the true level of noise in the measurements is somewhat obscured. To illustrate this, all measurements from both aircraft made above 1000 m a.s.l. have been removed and the resulting data-set is plotted as a function of data-point number, as opposed to time, so that the series plots are continuous (Figure S3). In addition, the x-axis limits for all subplots in Figure S3, regardless of the length of the flight, are identical. Figure S3 shows that the actual noise for both instruments is essentially comparable during most flights.

[27] A statistical comparison, at all altitudes and below 1000 m above sea level (a.s.l.) where local emissions influence BC concentrations most, between BC predictions and observations is given in Table 4. Although the extent of agreement between observations and predictions varies from flight to flight, the overall agreement (i.e. the 5-flight average) indicates that predicted BC concentrations have a slight positive bias (19.2%) when compared to P3 measurements below 1000 m a.s.l., and a significant positive bias (78.2%) when compared to Twin Otter measurements. Visual inspection of Figures 6–11 and Figures A1, A2, A3, A4 suggests that the CMAQ predictions capture the spatial distribution of BC during many flights, although the predicted concentration range is biased by 53 to 116% as compared to Twin Otter measurements below 1000 m a.s.l., and biased by -27% to 52% as compared to P3 measurements below 1000 m a.s.l. FLEXPART back trajectory analyses indicate that highest predicted BC concentrations exist in air masses influenced by emissions in the Long Beach industrial area. For example, the trajectory paths shown in Figure S4 suggest that during the 24 May flight, both observed and predicted concentrations of BC, at 11:21 (downtown Los Angeles) and 14:59 (Fontana), occurred in air masses that were influenced by emissions near Long Beach and downtown Los Angeles. We note that since WRF meteorological fields were used to drive FLEXPART, whereas MM5 meteorological fields were used to drive CMAQ, potential inconsistencies may exist between between the two sets of meteorology. Nevertheless, both the FLEXPART back trajectories and the extent of agreement between observed and predicted BC concentrations from both aircraft suggests that the locations of the BC sources are accurately accounted for in the CARB BC inventory used in this study.

[28] As mentioned previously, the calibration of the SP2 onboard the Twin Otter biased BC measurements low by 12% as compared to those of the SP2 onboard the P3 [*Metcalf et al.*, 2012]. Since the normalized statistical metrics used in this study are nonlinear functions of observed concentrations, the 12% measurement bias will cause higher than 12% bias when compared to predictions. As an example, in a 1-point data set, if the predicted BC concentration is 1 μg m^{-3} and the observed BC concentration is 0.568 μg m^{-3}, the NMB

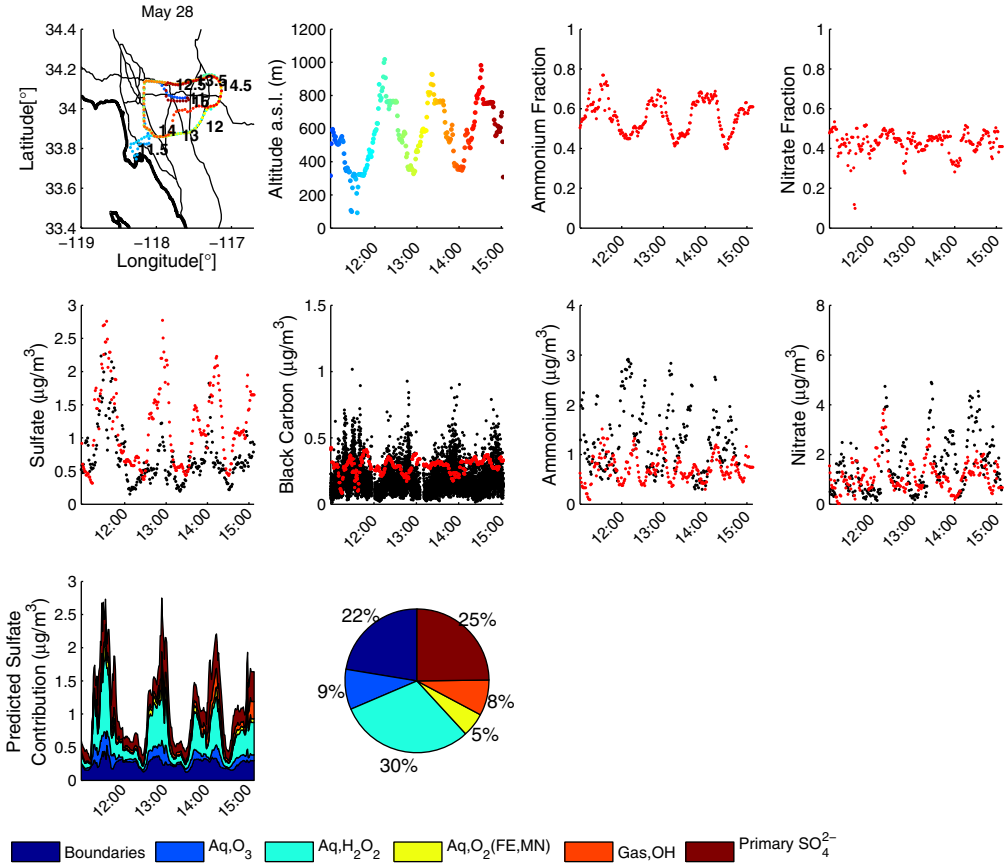

Figure 9. Same as Figure 6, but for the Twin Otter May 28 flight.

will be 76.1%. However, if the measured concentration is reduced to 0.5 μg m^{-3} due to the 12% instrument bias (88% of 0.568 is 0.5), the NMB becomes 100%, which is a difference inNMB of 23.9%. Taking this difference into account brings the NMBs from several of the Twin Otter flights into closer agreement with the higher NMBs from the P3 flight. For instance, dividing all Twin Otter measurements by 0.88 reduces the NMBs from the May 25, 27, and 28 Twin Otter flights (below 1000 m a.s.l.) to 56.5%, 34.6%, and 40.6%, respectively, making them comparable to the NMBs measured during the May 8 and 16 P3 flights, which are 52.3% and 39.5%, respectively. The precise reason for Twin Otter observations being a factor ~2 lower than predictions during the May 21 and 24 flights cannot be pinpointed at this time.

[29] Additional results showing measured and predicted CO mixing ratios (available only for P3 flights), as well as predicted and observed ΔBC/ΔCO ratios (Figure S5), are included in the Supplemental Material. For the comparison shown in Figure S5, ΔBC/ΔCO values are calculated by subtracting the minimum BC and CO measurements (background values) below 1000 m a.s.l. from all BC and CO measurements, respectively, below 1000 m a.s.l. Data points for which ΔCO < 1 ppbv are also removed. Note that, owing to data points lying on top of each other in Figure S5, the average ΔBC/ΔCO ratios (horizontal lines) can appear lower than the spread of individual data points may suggest. Since the accuracy of the ARCTAS-CARB CO emissions has already been established by *Wunch et al.* [2009], using measured and observed ratios of ΔBC/ΔCO reduces the impact of inaccuracies in meteorology at locations other than Pasadena. As shown in Figure S5, the comparisons of ΔBC/ΔCO are in general agreement with observations, with ratios being overpredicted during the May 8 and 16 flights, and underpredicted during the May 4, 14, and 16 flights. The agreement between surface measurements and the P3 measurements suggests that no systematic bias exists in the ARCTAS-CARB emission inventory, or the MM5 meteorology used in this study.

4.3. Sulfate

[30] To characterize the sources of the predicted sulfate, the CMAQ sulfate tracking system was employed, in which separate tracers are used to keep track of the sulfate contributions from the formation pathways listed in Table S1. Due to the transmission window of the AMS, the mass contributions from the Aitken mode and the coarse mode sulfate are a negligible fraction of the total predicted sulfate aerosol mass (< 1%) in the applicable size range and are not shown in Figure 4. Sulfate predicted to be formed by aqueous-phase oxidation by methyl hydrogen peroxide (MHP) and peroxyacetic acid (PAA) is also predicted to be negligible. However, *Stein and Saylor* [2012] show that the relative contributions of sulfate formation pathways depend critically on the chemical mechanism used. Specifically, during the ICARTT 2004 campaign, up to 30% of the sulfate in certain locations is attributable to the aqueous-phase oxidation of MHP when using CMAQv4.6 with the CBIV mechanism, and very little sulfate is attributable to PAA oxidation. However, this is likely

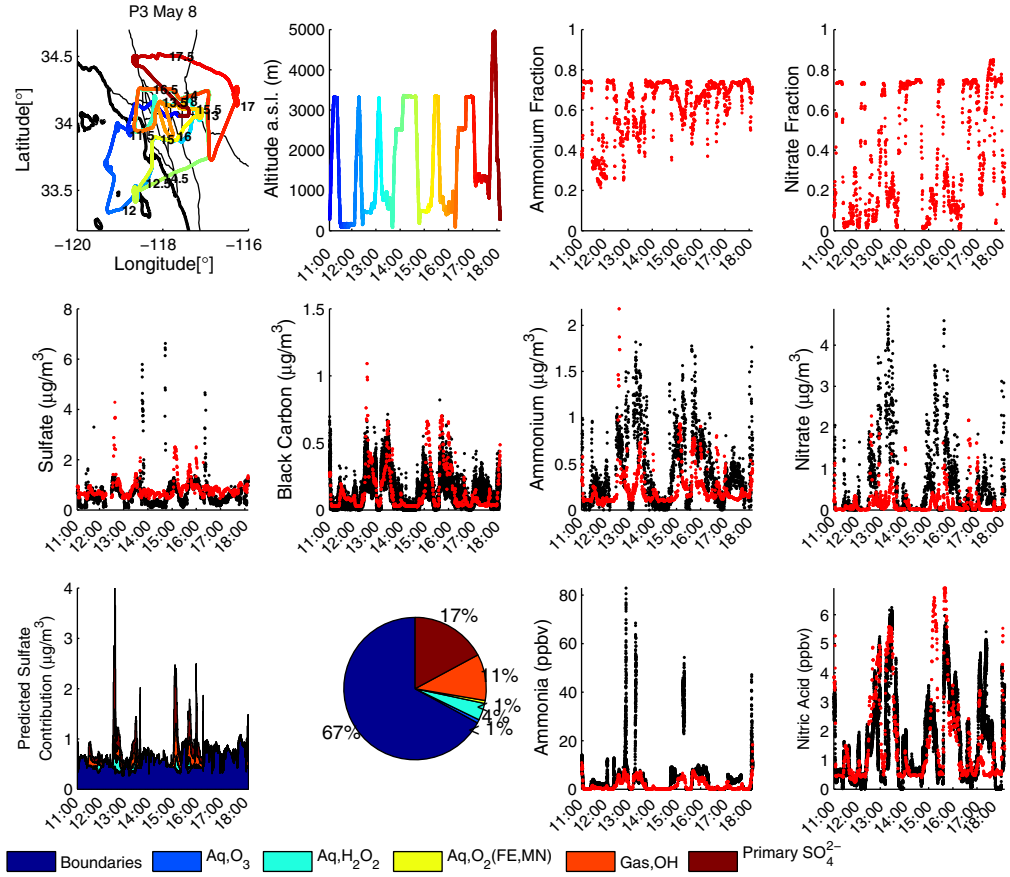

Figure 10. From left to right and top to bottom: P3 aircraft flight path for May 8, P3 altitudes (with respect to sea level) with the flight track and altitude trace are colored by the time (Pacific Standard Time) of day and time-stamps printed along each flight path in 30 min increments, Fraction of predicted particulate ammonium within the AMS transmission window, Fraction of predicted particulate nitrate within the AMS transmission window, predicted (red) and observed (black) sulfate concentrations, predicted (red) and observed (black) black carbon concentrations, predicted (red) and observed (black) nitrate concentrations, predicted (red) and observed (black) ammonium concentrations, predicted sulfate source apportionment, Pie chart indicating the relative contribution from routes to sulfate averaged over a given flight. In the bottom legend, "Boundaries" refers to sulfate attributable to boundary conditions, "(Aq,Gas),OX" refers to secondary sulfate produced by aqueous-phase (Aq) orgas-phase (Gas) oxidation of SO_2 by oxidant OX. "Primary SO_4^{2-}" refers to sulfate emitted within the basin.

an overestimation since the MHP concentrations were overpredicted by an order of magnitude with that mechanism. Furthermore, when using the CB05 or SAPRC99 mechanisms, very little sulfate is attributable to MHP oxidation, and up to 20% is attributable to PAA oxidation. However, this is also likely an overestimation since the PAA was overpredicted by up to a factor of 4 when using the CB05 or SAPRC99. We are not aware of any sulfate tracking assessments based on the SAPRC07 mechanism combined with the ARCTAS-CARB inventory. Although Fe^{3+} and Mn^{2+} are not model-predicted species in CMAQv4.7.1 (although they are in CMAQv5.0), prescribed background concentrations of 0.01 μg m^{-3} Fe^{3+} and 0.005 μg m^{-3} Mn^{2+} still lead to a small, but non-negligible, portion (up to 5%) of accumulation mode sulfate forming via these routes [*Walcek and Taylor*, 1986; *Chang et al.*, 1987]. The predominant predicted accumulation mode sulfate comes from four sources (no particular order): the inflow of sulfate from the boundaries (e.g. Asian inflow [*Lin et al.*, 2012]), aqueous-phase oxidation of S(IV) by H_2O_2 and O_3, gas-phase photooxidation of SO_2, and direct sulfate emission.

4.3.1. Pasadena Ground Site

[31] Observed and predicted sulfate and sulfur dioxide concentrations from the CalNex Pasadena ground site are shown in Figure 4, and statistical metrics are given in Table 1. In addition, ground-site SO_2 measurements from three locations within the L.A. Basin, taken from the CARB AQMIS are compared to CMAQ predictions in Figure 5. As at the Pasadena ground site, SO_2 mixing ratios are over-predicted at all locations within the L.A. Basin.

[32] Despite over-predictions in SO_2, predicted sulfate concentrations are actually biased low compared to sulfate measurements at the Pasadena ground site, mostly due to underestimations during the first few days of comparison. The relative sulfate contributions are listed in Table 5. Few clouds are present during daylight hours, but an MM5 predicted nighttime coastal marine layer facilitates aqueous-phase conversion of S(IV) to S(VI) in CMAQ. The predicted

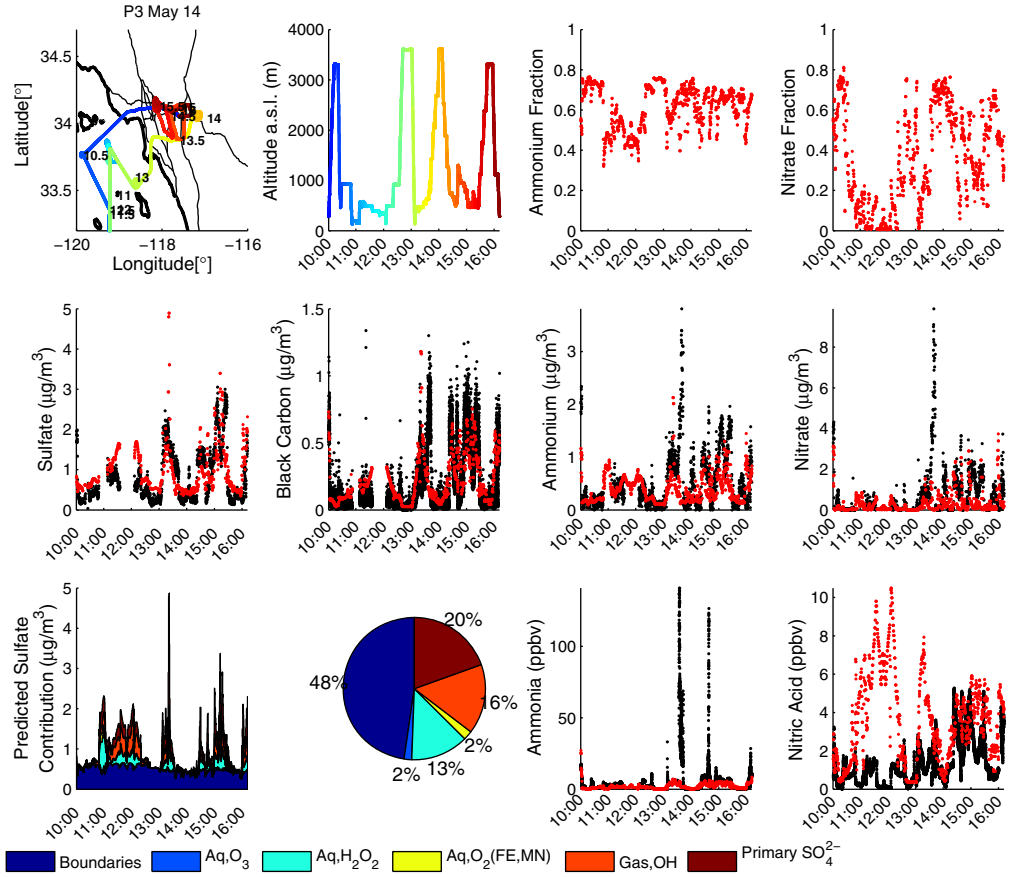

Figure 11. Same as Figure 10, but for the P3 May 14 flight.

marine layer evaporates during the day, but the cloud-processed sulfate remains airborne. At the Pasadena ground-site, enhancements in the relative sulfate contributions from aqueous-phase oxidation of SO_2 are not directly proportional to over-predictions in SO_2 emissions owing partially to the nonlinear pH dependence of the rate of S(IV) oxidation by O_3. More specifically, the second-order reaction rate constant for the S(IV)-O_3 reaction varies by up to four orders of magnitude for aerosol pH ranging from 1 to 6 [*Seinfeld and Pandis*, 2006]. Production of sulfate via this reaction lowers the pH and slows down the reaction. In addition, if the oxidants H_2O_2 and O_3 are the limiting reactants, the impacts of overestimated SO_2 emissions will also be lessened. Sulfate formation via gas-phase oxidation of SO_2 should respond more linearly to increases in SO_2 concentrations. However, the lifetime of SO_2 against the hydroxyl radical is relatively long (~1 week, *Seinfeld and Pandis* [2006]) and only represents 7% of the average predicted sulfate at the Pasadena ground site. Long-range transport of sulfate is predicted (CMAQ) to account for 26% of the sulfate measured at the Pasadena ground-site.

4.3.2. Twin Otter and P3

[33] Observed and predicted sulfate concentrations from the Twin Otter and P3 flights are shown in Figures 6–11 and Figures A1, A2, A3, A4. A statistical comparison between sulfate predictions and observations is given in Table 6. The average predicted sulfate concentration is biased high by 55% to 268% as compared to Twin Otter measurements, and biased by 0% to 71% as compared to P3 measurements

Table 2. Statistical Metrics Based on Measured and Predicted Temperature and Relative Humidity for Twin Otter and P3 Flights During May 2010

Flight Date	N	ME [°C]	MB [°C]
Temperature (Twin Otter)			
21	189	3.89	3.88
24	167	3.33	3.32
25	334	2.21	2.21
27	219	1.55	-1.23
28	239	0.75	-0.23
Temperature (P3)			
4	17219	2.12	0.60
8	25439	2.10	1.60
14	22258	3.77	3.33
16	27899	2.17	0.92
19	24239	1.67	0.71
Flight Date	N	ME [%]	MB [%]
Relative Humidity (Twin Otter)			
21	189	26.7	-26.6
24	167	9.99	-9.13
25	334	5.76	-5.12
27	219	10.5	5.67
28	239	7.16	-0.33
Relative Humidity (P3)			
4	17219	12.3	-0.47
8	25439	14.6	-1.00
14	22258	24.9	-22.1
16	27899	16.1	-7.91
19	24239	8.89	-2.49

ME = Mean Error, MB = Mean Bias. N is the number of data points collected during a given flight.

Table 3. Statistical Metrics Based on Measured and Predicted Wind Magnitudes and Directions for Twin Otter and P3 Flights During May 2010

Flight Date	N	ME [m/s]	MB [m/s]	NME	NMB
Wind Magnitudes (Twin Otter)					
21	180	1.89	1.19	0.38	0.23
24	167	1.79	-0.61	0.36	-0.12
25	334	1.89	0.49	0.37	0.10
27	219	2.04	0.98	0.56	0.27
28	239	2.00	2.11	0.55	0.52
Wind Magnitudes (P3)					
4	17219	2.33	-0.48	0.48	-0.10
8	25439	2.15	1.06	0.27	0.14
14	22258	1.69	0.57	0.55	0.19
16	27899	2.10	-0.26	0.41	-0.05
19	24239	4.03	-2.63	0.48	-0.31
Flight Date	N	ME [deg]	$\bar{\theta}_{obs}$ [deg]	$\bar{\theta}_{mod}$ [deg]	
Wind Directions (Twin Otter)					
21	180	23.8	242	254	
24	167	40.7	228	253	
25	334	28.8	209	223	
27	219	36.9	225	242	
28	239	22.5	240	246	
Wind Directions (P3)					
4	17219	64.0	263	239	
8	25439	24.2	263	276	
14	22258	65.1	203	206	
16	27899	54.5	224	230	
19	24239	25.2	278	267	

ME = Mean Error, MB = Mean Bias, NME = Normalized Mean Error, NMB = Normalized Mean Bias, and $\bar{\theta}$ = average wind direction. N is the number of data points collected during a given flight. The wind directions θ_{obs} and θ_{mod} are the observed and modeled wind directions, respectively, in units of degrees ($0^\circ \leq \theta \leq 360^\circ$). Wind direction, θ, is defined as the direction from which the wind is blowing, and is measured in degrees clockwise from true north.

Table 4. Statistical Metrics Based on Measured and Predicted Black Carbon Concentrations, at All Altitudes and Below 1000 m Above Sea Level, for Twin Otter Flights and P3 Flights During May 2010

Flight Date	N	ME [μg m^{-3}]	MB [μg m^{-3}]	NME	NMB
Black Carbon (Twin Otter, all altitudes)					
21	8537	0.23	0.19	1.08	0.90
24	6503	0.13	0.15	1.16	1.04
25	8256	0.13	0.11	0.84	0.70
27	8133	0.12	0.09	0.73	0.53
28	8700	0.14	0.11	0.79	0.60
5-flight average	40129	0.15	0.12	0.91	0.74
Black Carbon (Twin Otter, below 1000 m a.s.l.)					
21	6794	0.27	0.25	1.20	1.09
24	4117	0.17	0.16	1.26	1.16
25	5406	0.16	0.14	0.89	0.78
27	8133	0.12	0.09	0.73	0.53
28	8656	0.14	0.11	0.80	0.60
5-flight average	33106	0.17	0.14	0.94	0.78
Black Carbon (P3, all altitudes)					
4	16923	0.07	0.00	0.58	0.01
8	25257	0.08	0.04	0.74	0.32
14	18974	0.14	0.05	0.83	0.30
16	21273	0.10	0.07	1.32	1.01
19	23610	0.08	-0.03	0.47	-0.12
5-flight average	106037	0.09	0.03	0.79	0.31
Black Carbon (P3, below 1000 m a.s.l.)					
4	3527	0.13	-0.04	0.48	-0.13
8	11184	0.13	0.09	0.75	0.52
14	10803	0.16	0.02	0.62	0.09
16	9791	0.08	0.06	0.60	0.40
19	7518	0.17	-0.12	0.40	-0.27
5-flight average	42823	0.13	0.02	0.60	0.19

ME = Mean Error, MB = Mean Bias, NME = Normalized Mean Error, NMB = Normalized Mean Bias. N is the number of data points collected during a given flight.

(Table 6). Moreover, the relative contributions predicted from each sulfate source vary considerably for both aircraft depending on the individual flight path.

[34] A significant fraction of the predicted sulfate (airborne and ground-based) comes from direct sulfate emission and boundary inflow of sulfate, both of which are independent of SO_2 concentrations (Table 5 and Figures 6–11). That direct sulfate emission contributes a significant fraction of the predicted sulfate in the L.A. Basin can be understood via analysis of the CARB sulfur emission inventory (Tables S4 and S5). The CARB sulfur emission inventory includes gas-phase SO_2 emissions, gas-phase H_2SO_4 emissions, and particle-phase SO_4^{2-} emissions (i.e. direct sulfate emission). Since, sulfuric acid is highly water-soluble and has an extremely low vapor pressure, it is assumed to enter the particle-phase immediately upon emission. Therefore, direct sulfate emissions include both direct emission of sulfate and direct emission of sulfuric acid. The ratio (by mass) of the different sulfur emissions in the CARB inventory, $(H_2SO_4 + SO_4^{2-})/(H_2SO_4 + SO_4^{2-} + SO_2)$ within the Basin is ~5%. However, since only a fraction of the SO_2 emitted is converted to sulfate, the sulfate from primary emissions will account for more than 5% of the total sulfate measured at the ground site and by the aircraft [*Dominguez et al.*, 2008]. As shown in Figure 10 and 11, sharp increases in predicted sulfate were predicted but not measured by the P3 near Long Beach (e.g. 8 May just before 13:00 and 14 May just after 13:00). Similarly, FLEXPART back trajectories suggest that during the 21 May flight (at 11:23 and 13:57, specifically), the Twin Otter intercepted air masses that had been influenced by emissions near Long Beach (Figure S6) and should have contained high concentrations of primary sulfate. Since such hot spots of primary sulfate near Long Beach were generally not observed by the Twin Otter (Figures A1, 6, and 7), one concludes that the major source of disagreement between predicted and observed sulfate is most likely attributable to the emission inventory.

[35] Sulfate concentrations measured onboard the Twin Otter were below 1 μg m^{-3} on 21, 24, and 25 May and showed little spatial variation. For these three flights, the predicted sulfate attributable to the GEOS-Chem boundary conditions represents 43-58% of the total predicted sulfate and accounts for almost the entire measured sulfate. Boundary

Table 5. Relative Contributions to Predicted Sulfate Concentrations at the Pasadena Ground Site Averaged Over 15-30 May 2010

Sulfate Pathway	Predicted contribution (%)
Boundary inflow	26
Aq, O_3	6
Aq, H_2O_2	29
Aq, O_2 (FEMN)	4
Gas, OH	7
Primary SO_4^{2-}	28

"Boundary inflow" refers to sulfate attributable to boundary conditions, "(Aq,Gas),OX" refers to secondary sulfate produced by aqueous-phase (Aq) or gas-phase (Gas) oxidation of SO_2 by oxidant OX. "Primary SO_4^{2-}" refers to sulfate emitted within the basin. "FEMN" refers to catalysts Fe^{3+} and Mn^{2+}

Table 6. Statistical Metrics Based on Measured and Predicted Particulate Sulfate, Ammonium, and Nitrate Concentrations for Twin Otter and P3 Flights During May 2010

Twin Otter					
Flight Date	N	ME [$\mu g\ m^{-3}$]	MB [$\mu g\ m^{-3}$]	NME	NMB
Sulfate					
21	185	1.30	1.30	2.68	2.68
24	172	0.28	0.27	0.84	0.82
25	337	0.39	0.39	1.11	1.11
27	224	0.50	0.44	0.62	0.55
28	244	0.53	0.46	0.77	0.65
Ammonium					
21	185	0.92	-0.77	0.62	-0.52
24	172	0.29	-0.14	0.68	-0.33
25	337	0.54	-0.51	0.60	-0.56
27	224	0.59	-0.47	0.46	-0.36
28	244	0.42	-0.20	0.46	-0.22
Nitrate					
21	185	1.64	-1.47	0.73	-0.65
24	172	0.80	-0.50	0.84	-0.52
25	337	1.17	-0.94	0.72	-0.58
27	224	1.24	-0.85	0.52	-0.35
28	244	0.93	-0.37	0.61	-0.24
P3					
Flight Data	N	ME [$\mu g\ m^{-3}$]	MB [$\mu g\ m^{-3}$]	NME	NMB
Sulfate					
4	1722	0.26	0.24	0.79	0.71
8	2544	0.41	0.20	0.65	0.32
14	2226	0.47	0.16	0.59	0.20
16	2790	0.33	0.00	0.33	0.00
19	2424	0.20	0.02	0.33	0.02
Ammonium					
4	1722	0.23	-0.11	0.77	-0.36
8	2544	0.27	-0.17	0.65	-0.42
14	2226	0.33	-0.15	0.64	-0.28
16	2790	0.47	-0.38	0.65	-0.52
19	2424	0.70	-0.65	0.71	-0.65
Nitrate					
4	1722	0.50	-0.31	0.99	-0.62
8	2544	0.51	-0.38	0.93	-0.68
14	2226	0.62	-0.37	0.91	-0.55
16	2790	0.94	-0.77	0.94	-0.76
19	2424	2.03	-1.99	0.80	-0.78

inflow of sulfate affects predicted sulfate concentrations along P3 flight paths in a similar manner. That the sulfate boundary conditions exert a noticeable impact on sulfate concentrations within the basin is not totally unexpected. For instance, *Huang et al*. [2011] evaluated the inflow of sulfur oxides ($SO_x = SO_2 + SO_4^{2-}$) to the South Coast (SC) of California by comparing predictions from the STEM atmospheric chemical transport model against aircraft measurements during the ARCTAS-CARB campaign [*Jacob et al*., 2010] in June 2008. They estimated that elevated SO_x levels at altitudes between 1-4 km enhanced SO_4^{2-} surface levels by a maximum of ~0.13 ppb (0.13 ppb $SO_4^{2-} \simeq 0.5\ \mu g\ m^{-3}$ at 1 atmosphere and 300 K) during this time period. Despite the influence of long-range SO_x transport, *Huang et al*. [2011] found that near-surface SO_x concentrations were mostly influenced by local emissions and estimated that the 2005 CARB sulfur emissions were low by about a factor of two. This is in contrast to our findings which suggest that the 2008 CARB SO_2 emissions are overestimated (Figure 5). Since the sulfur emission inventory used in *Huang et al*. [2011] is similar to that used in this study, the most likely explanation is that SO_2 emissions have decreased from 2008 to 2010, which is consistent with sulfur emission regulations that went into effect during those two years.

[36] The CMAQ sulfate source apportionment presented in this study suggests that, with the current sulfur emission inventory based on emission factors from 2008, long-range transport of sulfate accounts for 22-82% of the sulfate in the L.A. Basin. However, if the reductions in sulfur emission factors reported by *Lack et al*. [2011] (~90%) were to be included in the simulations, unlike the results presented in *Huang et al*. [2011], the boundary inflow of sulfate would become the single largest contributor to predicted sulfate concentrations in the L.A. Basin. Future work should continue to quantify the impact of foreign and domestic emissions on Southern California air quality as this is crucial for determining the potential efficacy of emission control strategies, and establishing the necessity for international collaboration.

4.4. Ammonium and Nitrate

[37] Ammonium nitrate aerosol is semivolatile and continuously partitions between the gas- and aerosol-phase. The distributions of total ammonium ($NH_3 + NH_4^+$) and total nitrate ($NO_3^- + HNO_3$) between the gas- and aerosol-phases are sensitive to the relative concentrations of other ions such as sulfate, sodium, and chloride, as well as meteorological factors such as temperature and relative humidity.

4.4.1. Pasadena Ground Site

[38] Particulate ammonium and nitrate predictions are generally biased low at the Pasadena ground site (Table 1). Aside from the large over-prediction on 24 May, NH_3 concentrations are well predicted (average bias of 22%), and predicted HNO_3 concentrations have a 15-day average bias of -38%. *Nowak et al*. [2012] used observations from the P3 aircraft during CalNex to show that the NH_3 emissions from automobiles in the CARB inventory are fairly accurate and contribute ~60 metric tons day^{-1} to the NH_3 budget within the L.A. Basin. *Nowak et al*. [2012] also found the NH_3 emissions from dairy facilities in the eastern part of the L.A. Basin are likely understated by up to a factor of 20. Since, strictly during the daytime, the Pasadena ground site is downwind of downtown L.A., but upwind of the dairy facilities, the predicted and observed NH_3 at this location is represented well within CMAQ.

[39] Ground-site NO_x ($NO + NO_2$) measurements taken from the CARB AQMIS are compared to CMAQ predictions in Figure 5. NO_x mixing ratios are over-predicted by a factor of ~2 at the three locations (North Long Beach, L.A.Westchester, and L.A. North Main Street location). Although slight over-predictions of temperature and under-predictions of RH artificially shift particulate ammonium and nitrate to the gas-phase, both particulate nitrate and nitric acid concentrations are underpredicted from 15-20 May. Since SO_4^{2-}, HNO_3, NO_3^-, and NH_4^+ are underpredicted during the first week of comparison, but are in better agreement with predictions during the second week, and since these species have different upwind sources, it is likely that errors in predicted wind fields, as opposed to uncertainties in the CARB emission inventory, are responsible for disagreement during the first week of comparison. Uncertainties/inaccuracies in predicted sea-salt emissions may also influence the agreement between predictions and observations at the Pasadena ground site, as will be discussed in the next section.

Table 7. Statistical Metrics Based on Measured and Predicted Ammonia and Nitric Acid Mixing Ratios for P3 Flights During May 2010

P3					
Flight Date	N	ME [ppbv]	MB [ppbv]	NME	NMB
Nitric Acid					
4	17219	0.92	-0.54	0.46	-0.27
8	25439	0.86	0.15	0.56	0.09
14	22258	2.50	2.32	1.96	1.82
16	27899	0.60	0.09	0.41	0.06
19	24239	0.96	-0.31	0.46	-0.15
Ammonia					
4	17219	2.96	-2.00	0.81	-0.55
8	25439	3.37	-3.00	0.98	-0.60
14	22258	3.80	-3.11	0.72	-0.59
16	27899	2.78	-2.05	0.86	-0.63
19	24239	12.38	-12.31	0.91	-0.90
Ammonia (no dairy)					
4	17219	1.39	-0.15	0.78	-0.09
8	25439	2.17	-1.98	0.60	-0.55
14	22258	1.25	-0.83	0.47	-0.31
16	27899	0.82	-0.34	0.77	-0.32
19	24239	2.80	-2.73	0.67	-0.68

Statistical metrics based on ammonia measurements in the "no dairy" column are calculated excluding all data points east of longitude 117.7°W.

4.4.2. Twin Otter and P3

[40] Observed and predicted particulate nitrate and ammonium concentrations from the Twin Otter and P3 flights are shown in Figures 6–11 and Figures A1, A2, A3, A4. Statistical metrics for inorganic aerosol species from both aircraft are given in Table 6. The fraction of simulated mass the AMS would measure is determined by taking the ratio of predictions that have been modified to match the AMS transmission efficiency to the total, unmodified inorganic aerosol concentration predictions. As shown in Figures 6–11 and Figures A1, A2, A3, A4, application of the AMS transmission efficiency results in the removal of ∼35% of the total predicted particulate sulfate and ammonium, and 20-100% (higher removal at low altitudes where sea-salt is present) of the total predicted nitrate during all flights. Since all predicted inorganic components are assumed to be in a metastable state (i.e. an aqueous electrolyte solution), predicted coarse mode particulate nitrate forms when HNO_3 reversibly condenses onto coarse NaCl particles via solution thermodynamics [*Kelly et al*., 2010]. This causes a significant fraction of the predicted particulate nitrate to reside in the coarse aerosol mode, while ammonium and sulfate reside primarily within the accumulation mode. Since sea-salt emissions are modeled online in CMAQv4.7.1, variations in wind speed lead to fluctuations in sea-salt emissions, and therefore different distributions of nitrate between the accumulation mode and the coarse mode. As shown in Figure S7, the day-to-day differences in sodium emissions can be substantial. Therefore, the differences in the fraction of nitrate removed by the AMS transmission curve along somewhat similar flight paths is likely attributable to the amount of sea-salt emitted. For instance, the amount of predicted nitrate removed as a result of the AMS transmission efficiency curve is ∼40% on the 27 May flight and ∼55% on the 28 May flight, which is consistent with the sea-salt emissions on May 28 being much greater than on May 27 (Figure S7). Adding size-resolved sodium and nitrate measurements, up to 10 μm, at various monitoring sites in the L.A. Basin would help unravel the impacts of anthropogenic and natural emissions on inorganic aerosol formation.

[41] Gas-phase measurements of HNO_3 and NH_3 were not conducted on the Twin Otter, so one cannot determine based on that data set alone if discrepancies between particulate ammonium and nitrate observations and predictions are the result of errors in the NO_x ($NO + NO_2$) emissions, NH_3 emissions, or predictions of HNO_3 within the SAPRC07TC chemical mechanism. However, HNO_3 and NH_3 measurements were conducted onboard the P3 aircraft (Figures 10, 11 and Figures A2, A3 and Table 7). As stated previously, *Nowak et al*. [2012] estimated, via mass balance, that the NH_3 emissions from automobiles in the CARB inventory are consistent with their measurements (∼60 metric tons day^{-1}), but that the CARB inventory underestimates NH_3 emissions from dairy facilities by a factor of 3-20. By conducting a formal 3-D simulation, we not only corroborate the conclusions of *Nowak et al*. [2012], but also show that NH_3 mixing ratios can be under-predicted by factors as high as $10^2 - 10^3$ (Figure 16). Moreover, sharp increases in submicrometer ammonium and nitrate measurements downwind of dairy facilities (e.g. Figure 11 just before 14:00) can be attrib uted entirely to point-source dairy NH_3 emissions. As these sharp increases in ammonium and nitrate are consistently missed by predictions, severely underpredicted NH_3 emissions from dairy facilities is identified as the dominant source of measurement/model disagreement in the eastern L.A. Basin. Upwind of dairies, predicted NH_3 mixing ratios are in better agreement with observations (see "no dairy" metrics in Table 7). Similarly, HNO_3 mixing ratios are generally predicted well during the P3 flights (NME typically ∼0.5) with the most notable exception being 14 May between 11:00 and 12:00 when the aircraft flew off the coast. HNO_3 and NO_x contour maps (not shown) suggest that the over-predictions on 14 May are caused by overstated coastal NO_x emissions (Figure 5).

[42] Even though gas-phase measurements were not taken onboard the Twin Otter, the impact of understated ammonia emissions and underpredicted total nitrate concentrations can be seen in the particulate ammonium and nitrate measurements (Figures 6–8). For instance, as shown in Figures 6 and 7, particulate ammonium and nitrate concentrations are significantly under-predicted in the eastern part of the L.A. Basin before the Twin Otter flew into the outflow regions at 12:30 and 14:30 during the 21 May flight. These under-predictions are exacerbated by an under-prediction of RH by 26.6% (flight average, Table 2). Particulate ammonium and nitrate concentrations are also under-predicted in the eastern part of the L.A. Basin during the 24 (between 13:00 and 15:00), 25 (between 13:30 and 15:30), and 27 (just after every hour) flights. Both predicted and observed nitrate concentrations are ∼2 times higher in the eastern part of the L.A. Basin on 25 May as compared to 24 May. The differences in nitrate concentrations are potentially attributable to warmer temperatures and lower RHs (predicted and observed) that shift both predicted and observed particulate nitrate to the gas-phase during the 24 May flight.

[43] Given that surface-level NO_x concentrations are generally over-predicted (Figure 5), one might expect the total nitrate mixing ratios to be over-predicted. However, as shown in Figure S8 and given in Table S2, the predicted total nitrate mixing ratios (within the AMS transmission window) agree with observations to within 50% NME, but tend to be

Table 8. Speciation of Primary PM_{fine} and PM_{coarse} Emissions Into Ca^{2+}, K^+, and Mg^{2+}

Fine Mode Species	Reff et al. [2009]
Ca^{2+}	0.0386×A25J
K^+	0.0309×A25J
Mg^{2+}	0.00368×A25J
Coarse Mode Species	CMAQv5.0[1]
Ca^{2+}	0.0838×ASOIL + 0.0562×ACORS
K^+	0.0242×ASOIL + 0.0176×ACORS
Mg^{2+}	0.0000×ASOIL + 0.0032×ACORS

[1]ASOIL = 0.9× PM_{coarse}, ACORS = 0.1× PM_{coarse}, A25J = PM_{fine}

under-predicted. There are several potential explanations for this. (1) Since the daytime production of HNO_3 occurs via gas-phase oxidation of NO_2 ($OH + NO_2 \rightarrow HNO_3$), the predicted OH concentration, which is highly dependent on the concentrations of hydrocarbons and other oxidants, may be too low. (2) The rate of conversion of NO to NO_2, which is also highly dependent on the concentrations of hydrocarbons and other oxidants, may be limiting. (3) The nighttime heterogeneous reaction of N_2O_5 ($N_2O_5(g) + H_2O(s) \rightarrow 2HNO_3$) may be understated. (4) If the predicted particulate nitrate mass concentrations are correct, but the size distributions predicted by CMAQ are inaccurate, the amount of predicted particulate nitrate could be biased low once predictions are adjusted to match the size-dependent transmission efficiency of the AMS. (5) Inaccurate shifting of total nitrate from the particle phase to the gas phase for various potential reasons (e.g. over-predicted temperature, under-predicted RH, over-predicted SO_4^{2-} concentrations, under-predicted NH_3 emissions) may artificially enhance the removal of total nitrate from the system due to faster dry deposition rates for gas-phase HNO_3 [*Dzepina et al*., 2009]. (6) Coarse cations (either from sea-salt particles or crustal species from dust emissions) may significantly reduce HNO_3 concentrations via condensation of HNO_3 onto deliquesced particles to form non-refractory coarse nitrate [*Fountoukis et al*., 2009; *Hsu et al*., 2007; *Moya et al*., 2002; *Jacobson*, 1999].

[44] We focus on the possibilities (4) and (6) regarding total nitrate underpredictions and defer a detailed analysis regarding the extent to which the other four sources of inaccuracy/uncertainty impact the amount of total nitrate predicted as the subject of future work. We note, however, that positive temperature biases and negative RH biases (Table 2), as well as positive sulfate biases (Table 6) and negative ammonia biases (Table 7), suggest that several of these possible factors contribute to shifting of predicted particulate nitrate to the gas-phase, thereby artificially enhancing total nitrate removal via dry deposition. To examine the hypothesis that total nitrate concentrations are underpredicted during most flights due to inaccurate distribution of total nitrate between the gas-phase, the fine aerosol-phase, and the coarse aerosol-phase, we present statistical metrics for all five P3 flights (Table S2) with and without the AMS transmission curve applied to predictions. When the AMS transmission efficiency is taken into consideration, total nitrate concentrations are underpredicted during four of the five P3 flights by 0-42% (Table S2). However, when full transmission (i.e. all predicted particulate nitrate and gas-phase nitric acid) is assumed, total nitrate concentrations are still underpredicted by up to 33% during the 4, 16, and 19 May flights. Since coarse particles were not measured onboard the Twin Otter or P3, the accuracy of the coarse mode nitrate predictions cannot be assessed. However, by comparing predicted and observed concentrations of total nitrate, assuming full transmission (Table S2), we show that regardless of whether nitrate is predicted to form ammonium nitrate, nitric acid, or coarse nitrate (e.g. sodium nitrate, calcium nitrate, potassium nitrate, etc.), on most days predicted total nitrate concentrations are simply not high enough. We deduce that the two likeliest causes of this are: (1) there is a missing source of HNO_3, or (2) the inaccurate distribution of total nitrate between the gas-phase and the two aerosol modes artificially enhances the removal of nitrate via dry deposition.

4.4.3. Impact of Crustal Species on Ammonium and Nitrate

[45] Several studies have shown that crustal species (Mg^{2+}, K^+, Ca^{2+}), from both anthropogenic emissions and fugitive dust, can potentially influence the thermodynamic partitioning of ammonium and nitrate aerosol between the gas-phase and both fine and coarse aerosol modes [*Fountoukis et al*., 2009; *Moya et al*., 2002; *Jacobson*, 1999]. Dominant sources of crustal species include unpaved and paved roads, agricultural tilling, construction dust, and sand and gravel from mining and quarry operations [*Reff et al*., 2009]. Assessing the impacts of crustal species requires representation of fugitive dust emissions, anthropogenic dust emissions, and chemical speciation profiles to determine the mass fraction of crustal elements within the dust. All three of these inputs are not well constrained on regional and global scales. For example, in a modeling study of the April 2001 dust storm episode over the trans-Pacific domain, *Wang et al*. [2012] assume that 10% of emitted crustal species reside in the fine mode and 90% reside in the coarse mode based on results presented in *Midwest Research Institute*, 2005, and use a static speciation profile based on *Van Pelt and Zobeck* [2007] to map 0.10%, 0.17%, and 0.071% of fugitive dust to K^+, Ca^{2+}, and Mg^{2+}, respectively. In contrast, in CMAQv5.0, 80% of fugitive dust emissions are assumed to reside in the coarse mode and 20% in the fine mode. In CMAQv5.0, a static speciation profile is used to map 3.8%, 7.9%, and 0.0% of all windblown dust to K^+, Ca^{2+}, and Mg^{2+}, respectively (http://www.cmaq-model.org/cmaqwiki/index.php?title=CMAQv5.0_PMother_speciation), while fine mode soil dust requires source specific speciation profiles available from the EPA SPECIATE database (http://www.epa.gov/ttnchie1/software/speciate/). One concludes that simulating dust emissions of crustal species is quite uncertain. Despite this high uncertainty, the potential influence of crustal species on aerosol formation suggests that this be addressed, if only approximately.

[46] Crustal species are not represented explicitly in the standard CMAQv4.7.1 model, and the ARCTAS-CARB emission inventory does not contain speciated crustal emission rates. However, the ARCTAS-CARB emission inventory does include two species, PM_{fine} and PM_{coarse}, which represent primary, unspeciated, fine and coarse mode particulate emissions, respectively. Within CMAQv4.7.1, 90% of PM_{coarse} emissions are assigned to the inert species ASOIL, which represents all coarse-mode, soil-derived, fugitive dust emissions, and 10% are assigned to the inert species ACORS, which represents non-fugitive dust emissions from anthropogenic sources such as diesel trucks. All fine dust emissions are assigned to the unspeciated accumulation-mode species

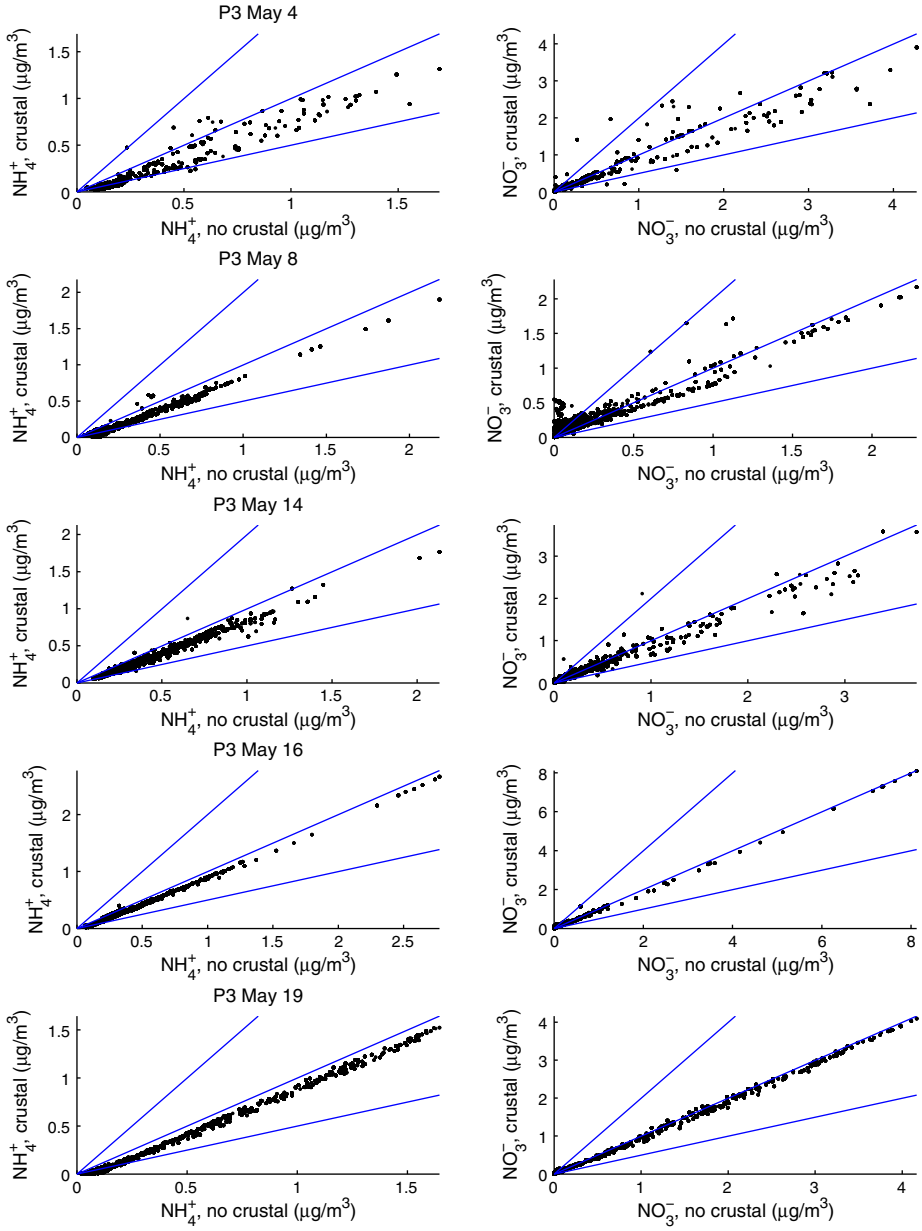

Figure 12. Scatter plots showing predicted ammonium and nitrate concentrations, with and without crustal species, along five P3 flight paths. Ammonium and nitrate predictions have been corrected to account for the transmission window of the AMS. The 1–1, 1–2, and 2–1 lines are included for reference.

A25J (A = aerosol, 25 = PM2.5, J = accumulation mode). Long-range transport of fine and coarse dust is accounted for via nested GEOS-Chem simulations of chemically inert dust species (http://wiki.seas.harvard.edu/geos-chem/index.php/Mineral_dust_aerosols).

[47] Due to a lack of information, we use static speciation profiles to assign the fractions of ACORS/ASOIL and A25J to coarse and fine mode crustal species, respectively (Table 8). Fine mode speciation profiles listed in Table 8 are taken directly from Figure 3 of *Reff et al*. [2009], and are based on average speciation profiles from the U.S. National Emission Inventory (2001). Coarse mode speciation profiles listed in Table 8 are taken directly from the static speciation profiles used in CMAQv5.0, which are based on a combination of speciation profiles from the EPA SPECIATE database. We have modified CMAQv4.7.1 to use ISORROPIAII, which allows for the inclusion of crustal species in thermodynamic calculations. We have not modified any other simulated processes (e.g. dry deposition, wet deposition, sea-salt emissions, aqueous-phase chemistry) to account for the chemical speciation of dust aerosol. As in the unmodified CMAQv4.7.1 model, mass is partitioned between the gas- and aerosol-phases according to the hybrid method [*Capaldo et al*., 2000]

[48] For the sake of brevity, we restrict our analysis of crustal species to the P3 flights. Figure 12 shows particulate (still corrected for AMS transmission window) predicted along P3 flight paths, with and without crustal species. The results suggest that, with the inclusion of crustal species,

ammonium concentrations consistently decrease, while nitrate concentrations can increase, decrease, or remain virtually unchanged. *Jacobson* [1999] showed that, depending on the environment (e.g. ammonia limited, nitric acid limited), coarse crustal species can increase, decrease, or have virtually no effect on the predicted amount of coarse-mode nitrate. Nitrate concentration increases are caused by crustal cations driving nitric acid into the particle phase to maintain charge balance. Nitrate concentration decreases are caused by crustal cations increasing mixed activity coefficients and driving ammonium nitrate aerosol into the gas phase. When these two effects roughly cancel each other, nitrate concentrations remain unchanged and ammonium also gets shifted to the gas phase, or to a different aerosol mode (e.g. coarse aerosol phase). Figure S9 shows time-series plots of Ca^{2+}, K^{+}, and Mg^{2+} concentrations predicted along the five P3 flight paths, as well as the amount of additional fine and coarse mode nitrate that could potentially be neutralized by the crustal cations. Using the speciation profile listed in Table 8, predicted coarse mode Ca^{2+} concentrations are typically higher than fine mode concentrations, fine and coarse mode K^{+} concentrations are comparable, and Mg^{2+} is present only in the fine aerosol mode. Since crustal species are predicted to be present in both fine and coarse modes, it is difficult to decouple the impacts aerosol modes have on each other. Overall, the inclusion of crustal species tends to decrease submicrometer ammonium aerosol, and increase or decrease submicrometer nitrate aerosol depending on the relative concentrations of dust. However, other than the May 4 P3 flight, the results presented in Figure 12 indicate that the impact of crustal species is not very substantial, most likely due to low crustal species concentrations predicted along the P3 flight paths. Moreover, these results would be even less pronounced if the speciation factors from *Van Pelt and Zobeck* [2007] were to be used since they are roughly an order of magnitude lower than those listed in Table 8. These results suggest that the exclusion of crustal species in thermodynamic calculations is not the dominant source of error between predicted and observed fine ammonium and nitrate concentrations. Future work should focus on acquiring chemically-resolved and size-resolved (up to 10 μm) measurements of crustal species, sea-salt, and nitrate.

5. Summary and Conclusions

[49] A detailed three-dimensional chemical transport model (CMAQ version 4.7.1), which contains state-of-the-science gas-phase chemistry and aerosol thermodynamics, was applied during the May 2010 CalNex campaign in the Los Angeles Basin. Boundary conditions were extracted from a nested global-scale GEOS-Chem model (version 9.1.1) simulation. Input meteorology and emission inventories were provided by the CARB. Inorganic and BC aerosol predictions were compared against the suite of ground-based and airborne measurements taken from various CIRPAS Twin Otter and WP-3D flights. The FLEXPART Lagrangian particle dispersion model is used to determine the trajectories of air parcels that reached the aircraft.

[50] Comparisons of predicted and observed BC measurements at the Pasadena ground site suggest that potentially large peaks in measured BC concentrations may be missed on any given day, owing most likely to inaccuracy in the predicted wind fields, but are generally represented well by CMAQ. BC predictions are consistently higher than observations onboard the Twin Otter, which is at least partially due to a systematic bias inherent to the SP2 onboard. However, predicted and observed BC concentrations and ΔBC/ΔCO ratios along P3 flight paths suggests that no systematic bias exists in the ARCTAS-CARB BC emission inventory or the MM5 meteorology.

[51] SO_2 concentrations are consistently overpredicted at surface sites, while the agreement between predicted and observed sulfate concentrations is variable. Sulfate is overpredicted by 55%-268% as compared to Twin Otter measurements, 0%-71% as compared to P3 measurements, and is actually under-predicted by 17% as compared to observations at the Pasadena ground site. The sulfate source apportionment presented in this study suggests that, with the current sulfur emission inventory based on emission factors from 2008, long-range transport of sulfate accounts for a substantial fraction (22-82%) of the sulfate in L.A. Basin. However, if the reductions in sulfur emission factors reported by *Lack et al.* [2011] ($\sim$90%) were to be included in simulations, unlike the results presented in *Huang et al.* [2011], the boundary inflow of sulfate would become the single largest contributor to predicted sulfate concentrations in the L.A. Basin.

[52] Severely underpredicted NH_3 emissions from dairy facilities are identified as the dominant source of measurement/model disagreement in the eastern L.A. Basin. By comparing predicted and observed concentrations of total nitrate, with and without applying the AMS transmission window, we show that, regardless of whether nitrate is predicted to form ammonium nitrate, nitric acid, or coarse nitrate (e.g. sodium nitrate, calcium nitrate, potassium nitrate, etc.), on most days predicted total nitrate concentrations are simply not high enough. We deduce that the two likeliest causes of this are: (1) there is a missing source of HNO_3, or (2) the inaccurate distribution of total nitrate between the gas-phase and the two aerosol modes artificially enhances the removal of nitrate via dry deposition. We estimate that, for most P3 flights, the exclusion of crustal species in thermodynamic calculations is not the dominant source of error between predicted and observed fine ammonium and nitrate concentrations. However, as stated previously, there is considerable uncertainty in all parameters used in the crustal sensitivity simulation, and we are reluctant to draw conclusions based on this study alone.

[53] This work, as part of the CalNex campaign, provides an up-to-date characterization of the inorganic and black carbon fraction of the Los Angeles Basin particulate matter. Adding gas-phase NH_3 measurements and size-resolved measurements, up to 10 μm, of nitrate and various cations (e.g. Na^{+}, Ca^{2+}, K^{+}, Mg^{2+}) to routine monitoring stations in the L.A. Basin would facilitate interpreting day-to-day fluctuations in fine and coarse inorganic aerosol greatly. Future work will focus on improving and assessing the treatment of anthropogenic and fugitive dust emissions, as well as characterizing the nature of organic aerosol formation and evolution in the Los Angeles Basin.

Appendix A: Additional Flights

[54] Appendix A contains Figures A1, A2, A3, and A4.

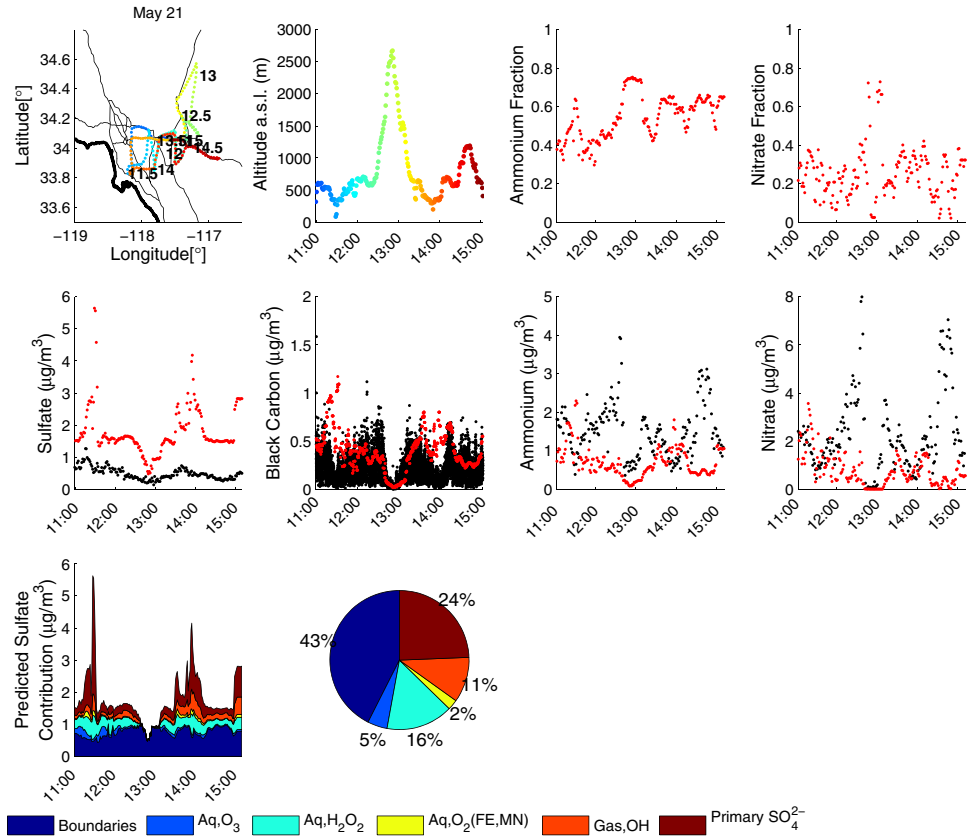

Figure A1. Same as Figure 6, but for the Twin Otter May 21 flight.

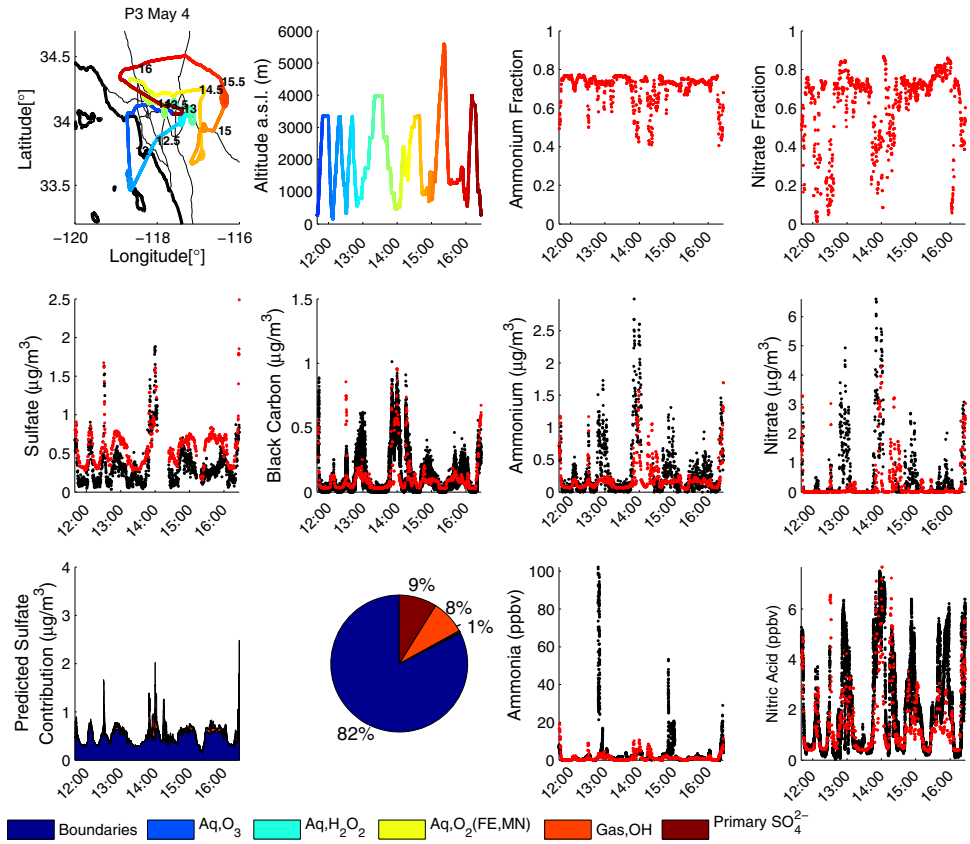

Figure A2. Same as Figure 10, but for the P3 May 4 flight.

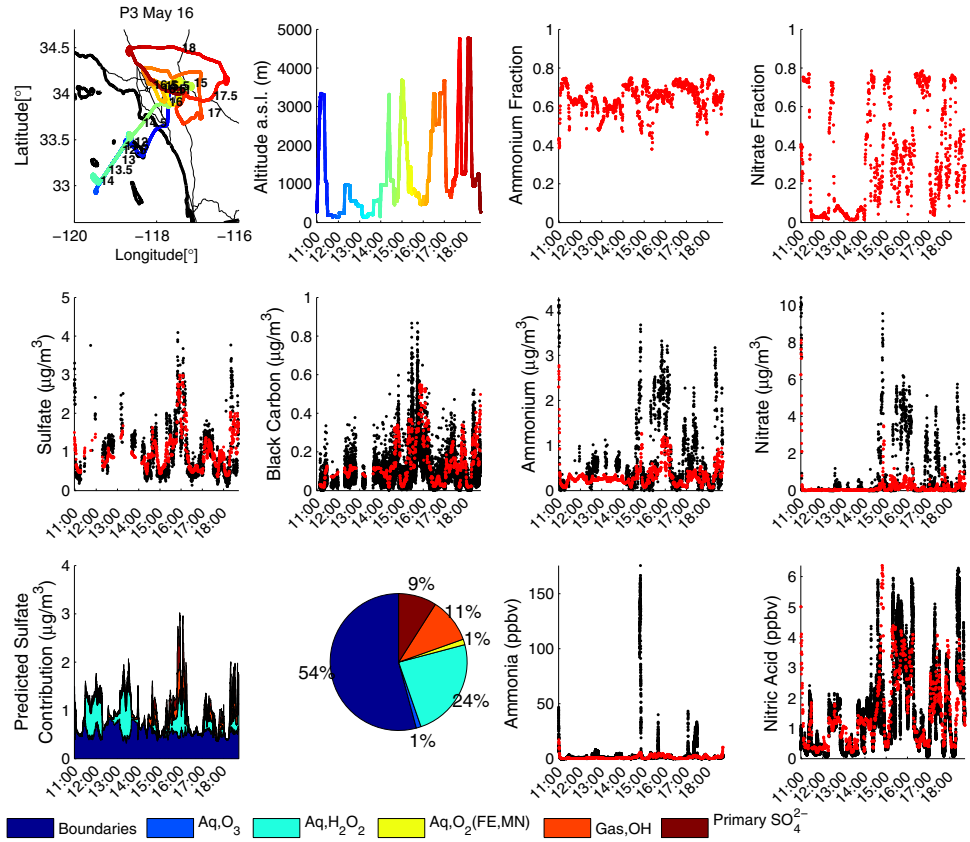

Figure A3. Same as Figure 10, but for the P3 May 16 flight.

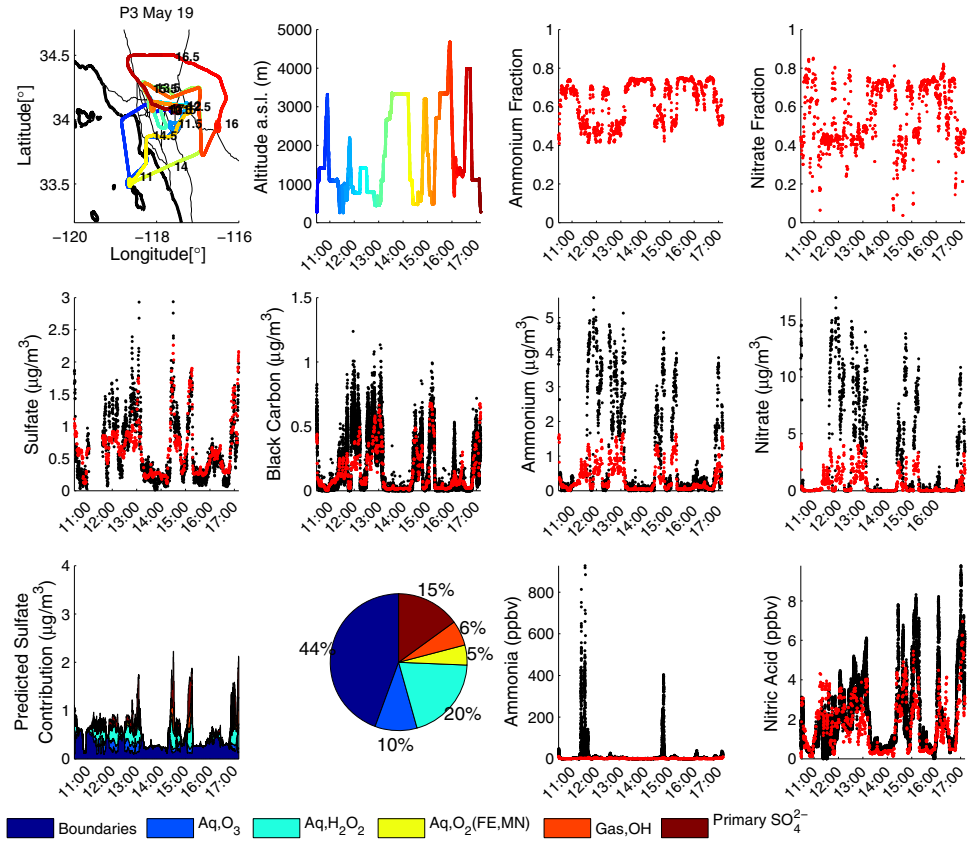

Figure A4. Same as Figure 10, but for the P3 May 19 flight.

Appendix B: AMS Transmission Efficiencies

[55] The AMS transmission curve used in this study is piece-wise defined for three diameter ranges: (a) linear increase in transmission vs ln(D_{va}), from 0% at D_{va} = 40 nm to 100% at D_{va} = 100 nm, (b) 100% transmission from D_{va} = 100 nm up to D_{va} = 550 nm, (c) linear decrease in transmission vs ln(D_{va}), from 100% at D_{va} = 550 nm to 0% at D_{va} = 2 μm, and zero elsewhere. This transmission curve can be applied analytically to any log-normal mass distribution:
40 nm < D_{va} < 100 nm:

$$f(D_{va}) = \frac{\ln(D_{va}/40nm)}{\ln(100nm/40nm)} \tag{B1}$$

$$\begin{aligned} &M(40\ nm < D_{va} < 100nm) = \\ &M(40\ nm/\rho_{dry} < D_p < 100\ nm/\rho_{dry}) = \\ &\frac{M_{tot}}{2} \times \frac{\ln\left(\bar{D}_{pgV}^{dry}/\left(40nm/\rho_{dry}\right)\right)}{\ln(100nm/40nm)} \\ &\quad \times \left[erf\left(\frac{ln\left(\left(100nm/\rho_{dry}\right)/\bar{D}_{pgV}^{dry}\right)}{\sqrt{2} \times \ln(\sigma_{dry})}\right) - erf\left(\frac{\ln\left(\left(40nm/\rho_{dry}\right)/\bar{D}_{pgV}^{dry}\right)}{\sqrt{2} \times \ln(\sigma_{dry})}\right)\right] + \\ &\frac{M_{tot}}{2} \times \frac{\ln(\sigma_{dry})}{\ln(100nm/40nm) \times \sqrt{\frac{\pi}{2}}} \times \left\{ \exp\left[-\left(\frac{\ln\left(\left(40nm/\rho_{dry}\right)/\bar{D}_{pgV}^{dry}\right)}{\sqrt{2} \times \ln(\sigma_{dry})}\right)^2\right] - \exp\left[-\left(\frac{\ln\left(\left(100nm/\rho_{dry}\right)/\bar{D}_{pgV}^{dry}\right)}{\sqrt{2} \times \ln(\sigma_{dry})}\right)^2\right]\right\} \end{aligned} \tag{B2}$$

100 nm < D_{va} < 550 nm:

$$f(D_{va}) = 1 \tag{B3}$$

$$\begin{aligned} &M(100\ nm < D_{va} < 550\ nm) \\ &= M\left(100\ nm/\rho_{dry} < D_p < 550\ nm/\rho_{dry}\right) \\ &= \frac{M_{tot}}{2} \times \left[erf\left(\frac{\ln\left(\left(550nm/\rho_{dry}\right)/\bar{D}_{pgV}^{dry}\right)}{\sqrt{2} \times \ln(\sigma_{dry})}\right) - erf\left(\frac{\ln\left(\left(100nm/\rho_{dry}\right)/\bar{D}_{pgV}^{dry}\right)}{\sqrt{2} \times \ln(\sigma_{dry})}\right)\right] \end{aligned} \tag{B4}$$

550 nm < D_{va} < 2000 nm:

$$f(D_{va}) = \frac{\ln(D_{va}/2000nm)}{\ln(550nm/2000nm)} \tag{B5}$$

$$M(550\ nm < D_{va} < 2000\ nm) = M\left(550\ nm/\rho_{dry} < D_p < 2000\ nm/\rho_{dry}\right) = \frac{M_{tot}}{2} \times \frac{\ln\left(\bar{D}_{pgV}^{dry}/\left(2000nm/\rho_{dry}\right)\right)}{\ln(550nm/2000nm)} \times \left[erf\left(\frac{\ln\left(\left(2000nm/\rho_{dry}\right)/\bar{D}_{pgV}^{dry}\right)}{\sqrt{2} \times \ln\left(\sigma_{dry}\right)}\right) - erf\left(\frac{\ln\left(\left(550nm/\rho_{dry}\right)/\bar{D}_{pgV}^{dry}\right)}{\sqrt{2} \times \ln\left(\sigma_{dry}\right)}\right)\right] + \frac{M_{tot}}{2} \times \frac{\ln\left(\sigma_{dry}\right)}{\ln(550nm/2000nm) \times \sqrt{\frac{\pi}{2}}} \times \left\{exp\left[-\left(\frac{\ln\left(\left(550nm/\rho_{dry}\right)/\bar{D}_{pgV}^{dry}\right)}{\sqrt{2} \times \ln\left(\sigma_{dry}\right)}\right)^2\right] - exp\left[-\left(\frac{\ln\left(\left(2000nm/\rho_{dry}\right)/\bar{D}_{pgV}^{dry}\right)}{\sqrt{2} \times \ln\left(\sigma_{dry}\right)}\right)^2\right]\right\} \quad \text{(B6)}$$

where f is the transmission efficiency as a function of D_{va}, M_{tot} is the unmodified, total amount of predicted species mass (e.g. nitrate, sulfate, ammonium) in the mode, and $M(D_{va,min} < D_{va} < D_{va,max})$ is the modified amount of species mass, within the mode, in the given vacuum-aerodynamic diameter range. The vacuum-aerodynamic diameter limits of the AMS transmission curve are converted to particle (Stokes) diameters for each data point by using $D_p = \left(\frac{\rho_o}{\rho_{dry}}\right) D_{va}$ [*DeCarlo et al.*, 2004], where D_p is the physical (Stokes) diameter of the particle, D_{va} is the vacuum-aerodynamic diameter, ρ_o is the standard density (1 g cm^{-3}), and ρ_{dry} is the density of the particle predicted by CMAQ not including water. The total mass from each mode (using this specific AMS transmission efficiency curve) is then:

$$M_{mode}^{AMS} = M(40\ nm < D_{va} < 100\ nm) + M(100\ nm < D_{va} < 550\ nm) + M(550\ nm < D_{va} < 2000\ nm) \quad \text{(B7)}$$

where M_{mode}^{AMS} is the total amount of predicted species mass in the mode that has been adjusted to match the transmission curve of the AMS. The total amount of predicted species mass that should be compared to the AMS is then the sum of all three adjusted modes ($M = M_I^{AMS} + M_J^{AMS} + M_K^{AMS}$), where I, J, and K are the Aitken mode, the accumulation mode, and the coarse mode, respectively. The derivation of the equations for transmission curve adjustment are presented in the supplementary section.

[56] **Acknowledgments.** This work was funded by NOAA grant NA09OAR4310128 and by the State of California Air Resources Board (CARB) Agreement 10-328. NOAA's Climate and Air Quality programs supported the NOAA-P3 deployment. PLH and JLJ were supported by CARB-319 and DOE (BER, ASR program) DE-SC0006035, and PLH acknowledges a CIRES Visiting Postdoctoral Fellowship. This work was supported in part by the NOAA Health of the Atmosphere Program and the NOAA Climate Goal. We acknowledge four anonymous reviewers for their thorough and insightful comments. The authors would like to thank Nehzat Motallebi, Havala O. T. Pye, and Andreas Zuend for useful discussions, Ying Xie and Rob Pinder at the Environmental Protection Agency (EPA) for providing the SAPRC07TC chemical mechanism, Anne Perring, Joshua Schwartz, and David Fahey for the use of the SP2 measurements from the NOAA P3 aircraft and for useful discussion, John Holloway at NOAA for CO measurements from the NOAA P3 aircraft, Kemal Gurer for MM5 modeled data, and Jerome Fast for providing the Aerosol Modeling Testbed analysis toolkit. The statements and conclusions in this paper are those of the researchers (contractor) and not necessarily those of CARB. The mention of commercial products, their source, or their use in connection with material reported herein is not to be construed as actual or implied endorsement of such products.

References

Appel, B., E. Hoffer, Y. Tokiwa, and E. Kothny (1982), Measurement of sulfuric-acid and particulate strong acidity in the Los-Angeles basin, *Atmos. Environ.*, *16*, 589–593, doi:10.1016/0004-6981(82)90168-8.

Bahreini, R., et al. (2009), Organic aerosol formation in urban and industrial plumes near Houston and Dallas, Texas, *J. Geophys. Res.-Atmos.*, *114*, doi:10.1029/2008JD011493.

Bein, K. J., Y. Zhao, N. J. Pekney, C. I. Davidson, M. V. Johnston, and A. S. Wexler (2006), Identification of sources of atmospheric PM at the Pittsburgh Supersite - Part II: Quantitative comparisons of single particle, particle number, and particle mass measurements, *Atmos. Environ.*, *40*, S424–S444, doi:10.1016/j.atmosenv.2006.01.064.

Bey, I., D. Jacob, R. Yantosca, J. Logan, B. Field, A. Fiore, Q. Li, H. Liu, L. Mickley, and M. Schultz (2001), Global modeling of tropospheric chemistry with assimilated meteorology, Model description and evaluation, *J. Geophys. Res.-Atmos.*, *106*, 23,073–23,095, doi:10.1029/2001JD000807.

Binkowski, F., and S. Roselle (2003), Models-3 community multiscale air quality (CMAQ) model aerosol component - 1. Model description, *J. Geophys. Res.-Atmos.*, *108*, doi:10.1029/2001JD001409.

Bond, T., and R. Bergstrom (2006), Light absorption by carbonaceous particles: An investigative review, *Aerosol. Sci. Tech.*, *40*, 27–67, doi:10.1080/02786820500421521.

Brioude, J., et al. (2009), Effect of biomass burning on marine stratocumulus clouds off the California coast, *Atmos. Chem. Phys.*, *9*, 8841–8856.

Cabada, J., S. Rees, S. Takahama, A. Khlystov, S. Pandis, C. Davidson, and A. Robinson (2004), Mass size distributions and size resolved chemical composition of fine particulate matter at the Pittsburgh supersite, *Atmos. Environ.*, *38*, 3127–3141, doi:10.1016/j.atmosenv.2004.03.004.

Canagaratna, M. R., et al. (2007), Chemical and microphysical characterization of ambient aerosols with the aerodyne aerosol mass spectrometer, *Mass SpectromRev.*, *26*, 185–222, doi:10.1002/mas.20115.

Capaldo, K., C. Pilinis, and S. Pandis (2000), A computationally efficient hybrid approach for dynamic gas/aerosol transfer in air quality models, *Atmos. Environ.*, *34*, 3617–3627.

Carter, W. P. L. (2010), Development of a condensed SAPRC-07 chemical mechanism, *Atmos. Environ.*, *44*, 5336–5345, doi:10.1016/j.atmosenv.2010.01.024, 2nd Biennial Conference on Atmospheric Chemistry Mechanisms, Air Quality Res Ctr, Davis, CA, DEC, 2008.

Chang, J., R. Brost, I. Isaksen, S. Madronich, P. Middleton, W. Stockwell, and C. Walcek (1987), A 3-dimensional eulerian acid deposition model - physics concepts and formulation, *J. Geophys. Res.-Atmos.*, *92*, 14,681–14,700, doi:10.1029/JD092iD12p14681.

Chow, J., E. Fujita, J. Watson, Z. Lu, D. Lawson, and L. Asbaugh (1994), Evaluation of filter-based aerosol measurements during the 1987 Southern California Air-Quality Study, *Env. Monit. Assess.*, *30*, 49–80, doi:10.1007/BF00546199.

Croes, B., and E. Fujita (2003), Overview of the 1997 Southern California Ozone Study (SCOS97-NARSTO), *Atmos. Environ.*, *37*, S3–S26, doi:10.1016/S1352-2310(03)00379-0.

Dallmann, T., R. Harley, and T. Kirchstetter (2011), Effects of diesel particle filter retrofits and accelerated fleet turnover on drayage truck

emissions at the port of oakland, *Environ. Sci. Technol.*, *45*, 10773–10779, doi:10.1021/es202609q.

de Foy, B., J. Varela, L. Molina, and M. Molina (2006), Rapid ventilation of the Mexico City basin and regional fate of the urban plume, *Atmos. Chem. Phys.*, *6*, 2321–2335.

DeCarlo, P., J. Slowik, D. Worsnop, P. Davidovits, and J. Jimenez (2004), Particle morphology and density characterization by combined mobility and aerodynamic diameter measurements. Part 1: Theory, *Aerosol. Sci. Tech.*, *38*, 1185–1205, doi:10.1080/027868290903907.

DeCarlo, P. F., et al. (2008), Fast airborne aerosol size and chemistry measurements above Mexico City and Central Mexico during the MILAGRO campaign, *Atmos. Chem. Phys.*, *8*, 4027–4048.

Ding, A., et al. (2009), Transport of north China air pollution by midlatitude cyclones: Case study of aircraft measurements in summer 2007, *J. Geophys. Res.-Atmos.*, *114*, doi:10.1029/2008JD011023.

Docherty, K. S., et al. (2011), The 2005 Study of Organic Aerosols at Riverside (SOAR-1): instrumental intercomparisons and fine particle composition, *Atmos. Chem. Phys.*, *11*, 12, 387-12, 420, doi:10.5194/acp-11-12387-2011, 2011.

Dominguez, G., T. Jackson, L. Brothers, B. Barnett, B. Nguyen, and M. H. Thiemens (2008), Discovery and measurement of an isotopically distinct source of sulfate in Earth's atmosphere, *Proc. Nat. Acad. Sci. USA*, *105*, 12 769–12 773, doi:10.1073/pnas.0805255105.

Drewnick, F., S. Hings, P. DeCarlo, J. Jayne, M. Gonin, K. Fuhrer, S. Weimer, J. Jimenez, K. Demerjian, S. Borrmann, and D. Worsnop (2005), A new time-of-flight aerosol mass spectrometer (TOF-AMS) - Instrument description and first field deployment, *Aerosol. Sci. Tech.*, *39*, 637–658, doi:10.1080/02786820500182040.

Dzepina, K., R. M. Volkamer, S. Madronich, P. Tulet, I. M. Ulbrich, Q. Zhang, C. D. Cappa, P. J. Ziemann, and J. L. Jimenez (2009), Evaluation of recently-proposed secondary organic aerosol models for a case study in Mexico City, *Atmos. Chem. Phys.*, *9*, 5681–5709, doi:10.5194/acp-9-5681-2009.

Eldering, A., G. Cass, and K. Moon (1994), An air monitoring network using continuous particle-size distribution monitors - connecting pollutant properties to visibility via mie scattering calculations, *Atmos. Environ.*, *28*, 2733–2749, doi:10.1016/1352-2310(94)90445-6.

Ellis, R. A., J. G. Murphy, E. Pattey, R. van Haarlem, J. M. O'Brien, and S. C. Herndon (2010), Characterizing a Quantum Cascade Tunable Infrared Laser Differential Absorption Spectrometer (QC-TILDAS) for measurements of atmospheric ammonia, *Atmos. Meas. Tech.*, *3*, 397–406, doi:10.5194/amt-3-397-2010.

Emeis, S. and K. Schafer (2006), Remote sensing methods to investigate boundary-layer structures relevant to air pollution in cities, *Bound.-Lay. Meteorol.*, *121*, 377–385, doi:10.1007/s10546-006-9068-2.

Fast, J., et al. (2009), Evaluating simulated primary anthropogenic and biomass burning organic aerosols during MILAGRO: implications for assessing treatments of secondary organic aerosols, *Atmos. Chem. Phys.*, *9*, 6191–6215, doi:10.5194/acp-9-6191-2009.

Fast, J. D., W. I. Gustafson, Jr., E. G. Chapman, R. C. Easter, J. P. Rishel, R. A. Zaveri, G. A. Grell and M. C. Barth (2011), The Aerosol Modeling Testbed: A community tool to objectively evaluate aerosol process modules, *Bull. Amer. Meteor. Soc.*, *92*, 343–360, doi:10.1175/2010BAMS2868.1.

Foley, K. M., et al. (2010), Incremental testing of the Community Multi-scale Air Quality (CMAQ) modeling system version 4.7, *Geosci. Mod. Devel.*, *3*, 205–226.

Fountoukis, C., and A. Nenes (2007), ISORROPIA II: a computationally efficient thermodynamic equilibrium model for K^+-Ca^{2+}-Mg^{2+}-NH_4^+-Na^+-SO_4^{2-}-NO_3^--Cl^--H_2O aerosols, *Atmos. Chem. Phys.*, *7*, 4639–4659.

Fountoukis, C., A. Nenes, A. Sullivan, R. Weber, T. Van Reken, M. Fischer, E. Matias, M. Moya, D. Farmer, and R. C. Cohen (2009), Thermodynamic characterization of Mexico City aerosol during MILAGRO 2006, *Atmos. Chem. Phys.*, *9*, 2141–2156.

Gong, S. (2003), A parameterization of sea-salt aerosol source function for sub- and super-micron particles, *Glo. Biogeochem. Cyc.*, *17*, doi:10.1029/2003GB002079.

Grell, G. A., J. Dudhia, and D. R. Stauffer (1995), A description of the fifth-generation Penn State/NCAR mesoscale model (MM5). NCAR Technical Note NCAR/TN-398+STR, Note TN398 STR, p. 138.

Haman, C. L. (2011), Seasonal and daily variability of the boundary layer and the impact of synoptic controls and micrometeorological processes on surface ozone evolution at an urban site, Ph.D. thesis, University of Houston, Texas, USA.

Hegg, D., D. Covert, H. Jonsson, and P. Covert (2005), Determination of the transmission efficiency of an aircraft aerosol inlet, *Aerosol Sci. Technol.*, *39*(10), 966–971, doi:10.1080/02786820500377814.

Holloway, J. S., R. O. Jakoubek, D. D. Parrish, C. Gerbig, A. Volz-Thomas, S. Schmitgen, A. Fried, B. Wert, B. Henry, and J. R. Drummond (2000), Airborne intercomparison of vacuum ultraviolet fluorescence and tunable diode laser absorption measurements of tropospheric carbon monoxide, *J. Geophys. Res.*, *105*(D19), 24,25124,261, doi:10.1029/2000JD900237.

Hsu, S.-C., S. C. Liu, S.-J. Kao, W.-L. Jeng, Y.-T. Huang, C.-M. Tseng, F. Tsai, J.-Y. Tu, and Y. Yang (2007), Water-soluble species in the marine aerosol from the northern South China Sea: High chloride depletion related to air pollution, *J. Geophys. Res.*, *112*, D19304, doi:10.1029/2007JD008844.

Huang, M., et al. (2011), Multi-scale modeling study of the source contributions to near-surface ozone and sulfur oxides levels over California during the ARCTAS-CARB period, *Atmos. Chem. Phys.*, *11*, 3173–3194, doi:10.5194/acp-11-3173-2011.

Hughes, L., J. Allen, L. Salmon, P. Mayo, R. Johnson, and G. Cass (2002), Evolution of nitrogen species air pollutants along trajectories crossing the Los Angeles area, *Environ. Sci. Technol.*, *36*, 3928–3935, doi:10.1021/es0110630.

Ianniello, A., F. Spataro, G. Esposito, I. Allegrini, M. Hu, and T. Zhu (2011), Chemical characteristics of inorganic ammonium salts in PM (2.5) in the atmosphere of Beijing (China), *Atmos. Chem. Phys.*, *11*, 10,803–10,822, doi:10.5194/acp-11-10803-2011.

Jacob, D. J., et al. (2010), The Arctic Research of the Composition of the Troposphere from Aircraft and Satellites (ARCTAS) mission: design, execution, and first results, *Atmos. Chem. Phys.*, *10*, 5191–5212, doi:10.5194/acp-10-5191-2010.

Jacobson, M. Z. (1999), Studying the effects of calcium and magnesium on size-distributed nitrate and ammonium with EQUISOLV II, *Atmos. Environ.*, *33*, 3635–3649, doi:10.1016/S1352-2310(99)00105-3.

Karydis, V. A., A. P. Tsimpidi, C. Fountoukis, A. Nenes, M. Zavala, W. Lei, L. T. Molina, and S. N. Pandis (2010), Simulating the fine and coarse inorganic particulate matter concentrations in a polluted megacity, *Atmos. Environ.*, *44*, 608–620, doi:10.1016/j.atmosenv.2009.11.023.

Kelly, J. T., P. V. Bhave, C. G. Nolte, U. Shankar and K. M. Foley (2010), Simulating emission and chemical evolution of coarse sea-salt particles in the Community Multiscale Air Quality (CMAQ) model, *Geosci. Mod. Devel.*, *3*, 257–273, doi:10.5194/gmd-3-257-2010.

Knote, C., et al. (2011), Towards an online-coupled chemistry-climate model: evaluation of trace gases and aerosols in COSMO-ART, *Geosci. Model Dev.*, *4*, 1077–1102, doi:10.5194/gmd-4-1077-2011.

Lack, D. A., et al. (2011), Impact of fuel quality regulation and speed reductions on shipping emissions: implications for climate and air quality, *Environ. Sci. Technol.*, *45*, 9052–9060, doi:10.1021/es2013424.

Lee, S. H., S. W. Kim, W. M. Angevine, L. Bianco, S. A. McKeen, C. J. Senff, M. Trainer, S. C. Tucker, and R. J. Zamora (2011), Evaluation of urban surface parameterizations in the WRF model using measurements during the Texas Air Quality Study 2006 field campaign, *Atmos. Chem. Phys.*, *11*, 2127–2143, doi:10.5194/acp-11-2127-2011.

Lin, M., et al. (2012), Transport of Asian ozone pollution into surface air over the western United States in spring, *J. Geophys. Res.-Atmos.*, *117*, doi:10.1029/2011JD016961.

Liu, D., K. Prather, and S. Hering (2000), Variations in the size and chemical composition of nitrate-containing particles in Riverside, CA, *Aerosol. Sci. Tech.*, *33*, 71–86, doi:10.1080/027868200410859.

Lu, R., and R. Turco (1995), Air pollutant transport in a coastal environment - II. 3-Dimensional simulations over Los-Angeles Basin, *Atmos. Environ.*, *29*, 1499–1518, doi:10.1016/1352-2310(95)00015-Q.

Luke, W. T. (1997), Evaluation of a commercial pulsed fluorescence detector for the measurement of low-level SO2 concentrations during GASIE. *J. Geophys. Res. 102*, 16, 25516, doi:10.1029/96JD03347.

Martucci, G., R. Matthey, V. Mitev, and H. Richner (2007), Comparison between backscatter lidar and radiosonde measurements of the diurnal and nocturnal stratification in the lower troposphere, *J. Atmos. Ocean. Technol.*, *24*, 1231–1244, doi:10.1175/JTECH2036.1.

Matsui, H., et al. (2009), Spatial and temporal variations of aerosols around Beijing in summer 2006: Model evaluation and source apportionment, *J. Geophys. Res.-Atmos.*, *114*, doi:10.1029/2008JD010906.

McKeen, S., et al. (2009), An evaluation of real-time air quality forecasts and their urban emissions over eastern Texas during the summer of 2006 Second Texas Air Quality Study field study, *J. Geophys. Res.-Atmos.*, *114*, doi:10.1029/2008JD011697.

McMeeking, G. R., et al. (2010), Black carbon measurements in the boundary layer over western and northern Europe, *Atmos. Chem. Phys.*, *10*, 9393–9414, doi:10.5194/acp-10-9393-2010.

Metcalf, A. R., J. S. Craven, J. J. Ensberg, J. Brioude, W. M. M. Angevine, A. Sorooshian, H. T. Duong, H. H. Jonsson, R. C. Flagan, and J. H. Seinfeld (2012), Black carbon aerosol over the Los Angeles Basin during CalNex, *J. Geophys Res.*, *117*, doi:10.1029/2011JD017255.

Middlebrook, A. M., R. Bahreini, J. L. Jimenez, and M. R. Canagaratna (2012), Evaluation of composition-dependent collection efficiencies for the Aerodyne Aerosol Mass Spectrometer using field data, *Aerosol. Sci. Tech.*, *46*, 258–271, doi:10.1080/02786826.2011.620041.

Midwest Research Institute (2005), Analysis of fine fraction of particulate matter in fugitive dust, Report to the WRAP by Midwest Research Institute, Project No. 110397.

Modey, W., D. Eatough, R. Anderson, D. Martello, S. Takahama, L. Lucas, and C. Davidson (2004), Ambient fine particulate concentrations and chemical composition at two sampling sites in metropolitan Pittsburgh: a 2001 intensive summer study, *Atmos. Environ.*, *38*, 3165–3178, doi:10.1016/j.atmosenv.2004.03.005.

Molina, L. T., et al. (2010), An overview of the MILAGRO 2006 Campaign: Mexico City emissions and their transport and transformation, *Atmos. Chem. Phys.*, *10*, 8697–8760, doi:10.5194/acp-10-8697-2010.

Moya, M., S. N. Pandis, and M. Z. Jacobson (2002), Is the size distribution of urban aerosols deter- mined by thermodynamic equilibrium?: An application to Southern California, *Atmos. Environ.*, *36*, 2349–2365, doi:10.1016/S1352-2310(01)00549-0.

Münkel, C., E. Noora, J. Räsänen, and A. Karppinen (2006), Retrieval of mixing height and dust concentration with lidar ceilometer, *Bound.-Lay. Meteorol.*, doi:10.1007/s10546-006-9103-3.

Murphy, S. M., et al. (2009), Comprehensive simultaneous shipboard and airborne characterization of exhaust from a modern container ship at sea, *Environ. Sci. Technol.*, *43*, 4626–4640, doi:10.1021/es802413j.

Neuman, J., et al. (2002), Fast-response airborne in situ measurements of HNO3 during the Texas 2000 Air Quality Study, *J. Geophys. Res.-Atmos.*, *107*, doi:10.1029/2001JD001437.

Neuman, J., et al. (2003), Variability in ammonium nitrate formation and nitric acid depletion with altitude and location over California, *J. Geophys. Res.-Atmos.*, *108*, doi:10.1029/2003JD003616.

Neuman, J. A., et al. (2012), Observations of ozone transport from the free troposphere to the Los Angeles basin, *J. Geophys. Res.-Atmos.*, *117*, doi:10.1029/2011JD016919.

Nolte, C. G., P. V. Bhave, J. R. Arnold, R. L. Dennis, K. M. Zhang, and A. S. Wexler (2008), Modeling urban and regional aerosols - Application of the CMAQ-UCD Aerosol Model to Tampa, a coastal urban site, *Atmos. Environ.*, *42*, 3179–3191, doi:10.1016/j.atmosenv.2007.12.059.

Nowak, J. B., J. A. Neuman, R. Bahreini, C. A. Brock, A. M. Middlebrook, A. G. Wollny, Holloway, J. S., Peischl, J., Ryerson, T. B., and F. C. Fehsenfeld (2010), Airborne observations of ammonia and ammonium nitrate formation over Houston, Texas, *J. Geophys. Res.-Atmos.*, *115*, doi:10.1029/2010JD014195.

Nowak, J. B., J. A. Neuman, R. Bahreini, A. M. Middlebrook, J. S. Holloway, S. A. McKeen, D. D. Parrish, T. B. Ryerson, and M. K. Trainer (2012), Ammonia sources in the California South Coast Air Basin and their impact on ammonium nitrate formation, *J. Geophys. Res.-Lett.*, *39*, doi:10.1029/2012GL051197.

Olivier, J. G. J., and J. J. M. Berdowski (2001), Global emissions sources and sinks. In: Berdowski, J., Guicherit, R. and B.J. Heij (eds.) The Climate System, pp. 33–78. A. A. Balkema Publishers/Swets and Zeitlinger Publishers, Lisse, The Netherlands., 2001.

Otte, T. L., and J. E. Pleim (2010), The Meteorology-Chemistry Interface Processor (MCIP) for the CMAQ modeling system: updates through MCIPv3.4.1, *Geosci. Model Dev.*, *3*, 243–256, doi:10.5194/gmd-3-243-2010.

Palau, J., G. Perez-Landa, J. Melia, D. Segarra, and M. Millan (2006), A study of dispersion in complex terrain under winter conditions using high-resolution mesoscale and Lagrangian particle models, *Atmos. Chem. Phys.*, *6*, 1105–1134.

Park, R., D. Jacob, B. Field, R. Yantosca, and M. Chin (2004): Natural and transboundary pollution influences on sulfate-nitrate-ammonium aerosols in the United States Implications for policy, *J. Geophys. Res.-Atmos.*, *109*, doi:10.1029/2003JD004473.

Parrish, D. D., et al. (2009), Overview of the Second Texas Air Quality Study (TexAQS II) and the Gulf of Mexico Atmospheric Composition and Climate Study (GoMACCS), *J. Geophys. Res.-Atmos.*, *114*, doi:10.1029/2009JD011842.

Pastor, S., J. Allen, L. Hughes, P. Bhave, G. Cass, and K. Prather (2003), Ambient single particle analysis in Riverside, California by aerosol time-of-flight mass spectrometry during the SCOS97-NARSTO, *Atmos. Environ.*, *37*, S239–S258, doi:10.1016/S1352-2310(03)00393-5.

Paulot, F., J. D. Crounse, H. G. Kjaergaard, J. H. Kroll, J. H. Seinfeld, and P. O. Wennberg (2009a), Isoprene photooxidation: new insights into the production of acids and organic nitrates, *Atmos. Chem. Phys.*, *9*, 1479–1501.

Paulot, F., J. D. Crounse, H. G. Kjaergaard, A. Kuerten, J. M. St Clair, J. H. Seinfeld, and P. O. Wennberg (2009b), Unexpected epoxide formation in the gas-phase photooxidation of isoprene, *Science*, *325*, 730–733, doi:10.1126/science.1172910.

Pekney, N. J., C. I. Davidson, K. J. Bein, A. S. Wexler, and M. V. Johnston (2006), Identification of sources of atmospheric PM at the Pittsburgh Supersite, Part I Single particle analysis and filter-based positive matrix factorization, *Atmos. Environ.*, *40*, S411–S423, doi:10.1016/j.atmosenv.2005.12.072.

Pfister, G. G., et al. (2011), Characterizing summertime chemical boundary conditions for airmasses entering the US West Coast, *Atmos. Chem. Phys.*, *11*, 1769–1790, doi:10.5194/acp-11-1769-2011.

Querol, X., et al. (2008), PM speciation and sources in Mexico during the MILAGRO-2006 Campaign, *Atmos. Chem. Phys.*, *8*, 111–128.

Reff, A., P. V. Bhave, H. Simon, T. G. Pace, G. A. Pouliot, J. D. Mobley, and M. Houyoux (2009), Emissions inventory of PM2.5 trace elements across the United States, *Environ. Sci. Technol.*, *43*, 5790–5796, doi:10.1021/es802930x.

Renner, E., and R. Wolke (2010), Modelling the formation and atmospheric transport of secondary inorganic aerosols with special attention to regions with high ammonia emissions, *Atmos. Environ.*, *44*, 1904–1912, doi:10.1016/j.atmosenv.2010.02.018.

Roberts, J. M., et al. (2010), Measurement of HONO, HNCO, and other inorganic acids by negative-ion proton-transfer chemical-ionization mass spectrometry (NI-PT-CIMS): Application to biomass burning emissions, *Atmos. Meas. Tech.*, *3*, 981–990, doi:10.5194/amt-3-981-2010.

Salcedo, D., et al. (2006), Characterization of ambient aerosols in Mexico City during the MCMA-2003 campaign with Aerosol Mass Spectrometry: results from the CENICA Supersite, *Atmos. Chem. Phys.*, *6*, 925–946.

Sarwar, G., and P. V. Bhave (2007), Modeling the effect of chlorine emissions on ozone levels over the eastern United States, *J. Appl. Met. Clim.*, *46*, 1009–1019, doi:10.1175/JAM2519.1.

Schafer, K., S. M. Emeis, A. Rauch, and C. Vogt (2004), Determination of mixing layer heights from ceilometer data, *Remote Sens. Clouds Atmos.*, *5571*, 248–259, doi:10.1117/12.565592.

Schwarz, J. P., et al. (2006), Single-particle measurements of midlatitude black carbon and light-scattering aerosols from the boundary layer to the lower stratosphere, *J. Geophys. Res.-Atmos.*, *111*, doi:10.1029/2006JD007076.

Schwarz, J. P., et al. (2008b), Coatings and their enhancement of black carbon light absorption in the tropical atmosphere, *J. Geophys. Res.-Atmos.*, *113*, doi:10.1029/2007JD009042.

Shiraiwa, M., Y. Kondo, N. Moteki, N. Takegawa, L. K. Sahu, A. Takami, S. Hatakeyama, S. Yonemura, and D. R. Blake (2008), Radiative impact of mixing state of black carbon aerosol in Asian outflow, *J. Geophys. Res.-Atmos.*, *113*, D24210, doi:10.1029/2008JD010546.

Seinfeld, J., and S. Pandis (2006), Atmospheric chemistry and physics: from air pollution to climate change (Second Edition), John Wiley and Sons, Inc..

Stein, A. F., and R. D. Saylor (2012), Sensitivities of sulfate aerosol formation and oxidation pathways on the chemical mechanism employed in simulations. *Atmos. Chem. Phys.*, *12*, 8567–8574, doi:10.5194/acp-12-8567-2012.

Stohl, A., C. Forster, A. Frank, P. Seibert, and G. Wotawa (2005), Technical note: The Lagrangian particle dispersion model FLEXPART version 6.2, *Atmos. Chem. Phys.*, *5*, 2461–2474.

Turpin, B., and J. Huntzicker (1991), Secondary formation of organic aerosol in the Los Angeles Basin - A descriptive analysis of organic and elemental carbon concentrations, *Atmos. Environ.*, *25*, 207–215, doi:10.1016/0960-1686(91)90291-E.

van der Kamp D., and I. McKendry (2010), Diurnal and seasonal trends in convective mixed-layer heights estimated from two years of continuous ceilometer observations in Vancouver, BC, *Bound.-Lay. Meteorol.*, *137*, 459475, doi:10.1007/s10546-010-9535-7.

Van Pelt, R. S., and T. M. Zobeck (2007), Chemical constituents of fugitive dust, *Environ. Monit. Assess.*, *130*, 3–16, doi:10.1007/s10661-006-9446-8.

van Pinxteren, D., E. Brueggemann, T. Gnauk, Y. Iinuma, K. Mueller, A. Nowak, P. Achtert, A. Wiedensohler, and H. Herrmann (2009), Size- and time-resolved chemical particle characterization during CAREBeijing-2006: Different pollution regimes and diurnal profiles, *J. Geophys. Res.-Atmos.*, *114*, doi:10.1029/2008JD010890.

Wang, K., Y. Zhang, A. Nenes, and C. Fountoukis (2012), Implementation of dust emission and chemistry into the Community Multiscale Air Quality modeling system and initial application to an Asian dust storm episode *Atmos. Chem. Phys. Disc.*, http://www.atmos-chem-phys-discuss.net/12/13457/2012/acpd-12-13457-2012-discussion.html.

Walcek, C., and G. Taylor (1986), A theoretical method for computing vertical distributions of acidity and sulfate production within cumulus clouds, *J. Atmos. Sci.*, *43*, 339–355, doi:10.1175/1520-0469(1986)043<0339:ATMFCV>2.0.CO;2.

Washenfelder, R. A., et al. (2010), Characterization of NO(x), SO(2), ethene, and propene from industrial emission sources in Houston, Texas, *J. Geophys. Res.-Atmos.*, *115*, doi:10.1029/2009JD013645.

Watson, J., J. Chow, Z. Lu, E. Fujita, D. Lowenthal, D. Lawson, and L. Ashbaugh (1994), Chemical mass-balance source apportionment of pm(10) during the Souther California air-quality study, *Aerosol. Sci. Tech.*, *21*, 1–36, doi:10.1080/02786829408959693.

Wittig, A., N. Anderson, A. Khlystov, S. Pandis, C. Davidson, and A. Robinson (2004), Pittsburgh air quality study overview, *Atmos. Environ.*, *38*, 3107–3125, doi:10.1016/j.atmosenv.2004.03.003.

Wunch, D., P. O. Wennberg, G. C. Toon, G. Keppel-Aleks, and Y. G. Yavin (2009), Emissions of greenhouse gases from a North American megacity, *Geophys. Res. Lett.*, *36*, L15810, doi:10.1029/2009GL039825.

Yue, D., et al. (2009), Characteristics of aerosol size distributions and new particle formation in the summer in Beijing, *J. Geophys. Res.-Atmos.*, *114*, doi:10.1029/2008JD010894.

Yue, D. L., et al. (2010), The roles of sulfuric acid in new particle formation and growth in the mega-city of Beijing, *Atmos. Chem. Phys.*, *10*, 4953–4960, doi:10.5194/acp-10-4953-2010.

Zhang, Y., P. Liu, B. Pun, and C. Seigneur (2006), A comprehensive performance evaluation of MM5-CMAQ for the Summer 1999 Southern Oxidants Study episode - Part I: Evaluation protocols, databases, and meteorological predictions, *Atmos. Environ.*, *40*, 4825–4838, doi:10.1016/j.atmosenv.2005.12.043.

Zhang, H., and Q. Ying (2010), Source apportionment of airborne particulate matter in Southeast Texas using a source-oriented 3D air quality model, *Atmos. Environ.*, *44*, 3547–3557, doi:10.1016/j.atmosenv.2010.06.004.

Zhang, J., W. Chameides, R. Weber, G. Cass, D. Orsini, E. Edgerton, P. Jongejan, and J. Slanina (2002), An evaluation of the thermodynamic equilibrium assumption for fine particulate composition. Nitrate and ammonium during the 1999 Atlanta Supersite Experiment, *J. Geophys. Res.-Atmos.*, *108*, doi:10.1029/2001JD001592.

Zheng, J., et al. (2011), Measurements of gaseous H(2)SO(4) by AP-ID-CIMS during CAREBeijing 2008 Campaign, *Atmos. Chem. Phys.*, *11*, 7755–7765, doi:10.5194/acp-11-7755-2011.